Received March 27, 2021, accepted April 9, 2021, date of publication April 13, 2021, date of current version April 23, 2021.

Digital Object Identifier 10.1109/ACCESS.2021.3072959

Online Parameter Estimation for Permanent Magnet Synchronous Machines: An Overview

Z. Q. ZHU[1], (Fellow, IEEE), DAWEI LIANG[1], AND KAN LIU[2], (Senior Member, IEEE)

[1]Department of Electronic and Electrical Engineering, The University of Sheffield, Sheffield S1 3JD, U.K.
[2]College of Mechanical and Vehicle Engineering, Hunan University, Changsha 410082, China

Corresponding author: Z. Q. Zhu (z.q.zhu@sheffield.ac.uk)

This work was supported by the U.K. Engineering and Physical Sciences Research Council (EPSRC) Prosperity Partnership "A New Partnership in Offshore Wind" under Grant EP/R004900/1.

ABSTRACT Online parameter estimation of permanent magnet synchronous machines is critical for improving their control performance and operational reliability. This paper provides an overview of the recent achievements of online parameter estimation of PMSMs with examples. The critical issues in parameter estimation are firstly analysed, especially the rank-deficient issue and inverter nonlinearities. Then, the state-of-the-art online parameter estimation modelling techniques are reviewed and assessed. Finally, some typical applications and examples are outlined, e.g. estimation of mechanical parameters, improvement of sensored and sensorless control performance, thermal condition monitoring, and fault diagnosis, together with future research trends.

INDEX TERMS Condition monitoring, control performance, electrical parameter, fault diagnosis, mechanical parameter, online parameter estimation, permanent magnet synchronous machine, sensorless control.

ACRONYMS

ADC	Analog-to-digital converter
AI	Artificial intelligence
ANN	Adaline neural network
AO	Adaptive observer
DO	Disturbance observer
DTC	Direct torque control
DWT	discrete wavelet transfer
EKF	Extended Kalman filter
EV/HEV	Electric/hybrid electric vehicle
FCS	Finite control set-model
FFT	Fast Fourier transform
FEA	Finite element analysis
FOC	Field oriented control
GA	Genetic algorithm
GPU	Graphics processing unit
HF	High frequency
ITSC	Inter-turn short-circuit
IPMSM	Interior PMSM
LMS	Least mean square
LPF	Low-pass filter
MPC	Model predictive control
MRAS	Model reference adaptive system
MTPA	Maximum torque per ampere
MTPV	Maximum torque per voltage
PF	Particle filter
PMSM	Permanent magnet synchronous machine
POPE	Position-offset based parameter estimation
PSO	Particle swarm optimization
PWM	Pulse width modulation
QGA	Quantum genetic algorithm
RLS	Recursive least square
SLPSO	Self-learning PSO
SMO	Sliding-mode observer
SPMSM	Surface-mounted PMSM
SNR	Signal-to-noise ratio
VSI	Voltage source inverter

The associate editor coordinating the review of this manuscript and approving it for publication was Shihong Ding.

I. INTRODUCTION

Due to high torque density and efficiency, permanent magnet synchronous machines (PMSMs) have been widely used in various applications [1], e.g. aerospace, domestic appliances, electric/hybrid electric vehicles (EV/HEV), servo drives, and wind power generation. In most industrial applications it is critical to acquiring accurate electrical and mechanical parameters for either improving control performance or achieving reliable fault diagnosis [2]–[8].

On the one hand, electrical parameters, i.e. stator resistance, inductance and rotor flux linkage, are essential in

various PMSM control strategies. More specifically, in EV/HEV and wind power applications, accurate electrical parameters are necessary to determine the optimal current trajectories under maximum torque per ampere (MTPA) and maximum torque per voltage (MTPV) strategies [9]–[17]. For the most common control methods, i.e. field-oriented control (FOC) [18]–[22], direct torque control (DTC) [23]–[26], as well as the model predictive control (MPC), [27]–[31], the accurate PMSM parameters are usually critical to ensuring system stability, improving efficiency and dynamic response. On the other hand, the mechanical parameters, e.g. moment of inertia and viscous friction coefficients, vary significantly with mechanical loads and are important in the design of speed-loop controllers [35]–[43].

In the last few decades, the techniques of parameter estimation have been extensively developed and the parameter estimation can be implemented, both offline and online. Generally, offline estimation is essential both in the machine and controller design and has been extensively used and investigated. In comparison, the online estimation method is primarily concerned with real-time acquiring electrical and mechanical parameters. The offline estimation methods have been well reviewed in [44] based on the time and frequency domains, as well as computational methods, i.e. finite element analysis (FEA), numerical, observer- and artificial intelligence (AI) -based methods. However, online methods are only very briefly outlined without reviewing the critical literature. Meanwhile, [45] focuses on the review of stator inductance estimation, including offline measurement at standstill and some online estimation algorithms, i.e. recursive least square (RLS), model reference adaptive system (MRAS), artificial neural network (ANN) and extended Kalman filter (EKF), however, no examples of online estimation algorithms were provided as part of the review. Thus, online parameter estimation techniques and associated critical issues have not been reviewed and assessed systematically so far.

This paper presents a comprehensive overview of online parameter estimation techniques, together with applications with extensive examples. The state-of-the-art techniques of online and offline parameter estimation are outlined in Section II. Section III describes the basis of PMSMs and drive systems, and emphasizes the general issues in parameter estimation. The widely used modelling techniques for online parameter estimation are introduced and assessed in Section IV, and the literature is summarized in Section V. Section VI introduces some typical industrial applications of online parameter estimation. Section VII prospects further research trends in this field. Section VIII concludes the paper.

II. OUTLINE OF THE STATE-OF-THE-ART TECHNIQUES OF PARAMETER ESTIMATION FOR PMSMS

A. PMSM MACHINE PARAMETERS

In general, the PMSM model can be expressed as [46]:

$$u_d = R_s(T_s)i_d + L_d^{inc}\frac{di_d}{dt} + L_{dq}^{inc}\frac{di_q}{dt} - \omega_r\psi_q, \quad (1a)$$

$$u_q = R_s(T_s)i_q + L_q^{inc}\frac{di_q}{dt} + L_{qd}^{inc}\frac{di_d}{dt} + \omega_r\psi_d, \quad (1b)$$

where

$$\psi_d = L_d\left(i_d, i_q\right)i_d + L_{dq}\left(i_d, i_q\right)i_q + \psi_q(i_d, i_q, T_{pm}), \quad (2a)$$

$$\psi_q = L_q(i_d, i_q)i_q + L_{qd}(i_d, i_q)i_d, \quad (2b)$$

where u_d, u_q, i_d, i_q are the dq-axis voltages and currents. R_s and ψ_q are the stator resistance and the rotor flux linkage at temperatures T_s and T_{pm}.ω_r is the electrical rotor speed. L_d^{inc}, L_q^{inc}, L_{dq}^{inc}, L_{qd}^{inc}, L_d, L_q, L_{dq} and L_{qd} are the dq-axis incremental and apparent self- and mutual-inductances, respectively.

As is well known, temperatures have a significant influence on stator resistance and rotor flux linkage, while the magnetic saturation also significantly affects rotor flux linkage and dq-axis stator inductances, respectively.

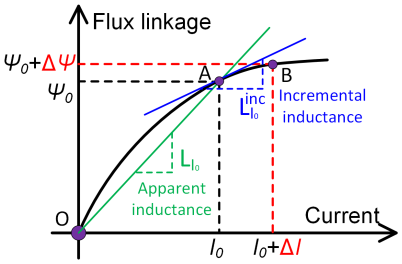

FIGURE 1. Illustration of incremental and apparent inductances.

On the one hand, the incremental inductance L^{inc} is defined as the slope at the operating point (3), while the apparent inductance L^a is defined as the flux linkage divided by current (4), which are graphically illustrated in Fig. 1. When the magnetic circuit is unsaturated, the incremental inductances are the same as the apparent inductances, whereas incremental inductances become smaller once the magnetic circuit is saturated due to nonlinear change of flux linkage with current.

$$L^{inc} = \frac{\partial\psi}{\partial i}, \quad (3)$$

$$L^a = \frac{\psi}{i}. \quad (4)$$

On the other hand, the cross-coupling effect also exists. The increase of q-axis current deepens the magnetic saturation level, which in turn will lead to a decrease in d-axis inductance. Likewise, the cross-coupling effect of d-axis current on the q-axis inductance is the same.

In [90], the relationship between the incremental and apparent inductances is established. The dq-axis incremental inductance matrix $\boldsymbol{L}_{\boldsymbol{dq}}^{\boldsymbol{inc}}$ is adjusted to the diagonal matrix $\boldsymbol{L}_{\boldsymbol{dq,adj}}^{\boldsymbol{inc}}$, i.e.

$$\boldsymbol{L}_{\boldsymbol{dq}}^{\boldsymbol{inc}} = \begin{bmatrix} L_d^{inc} & L_{dq}^{inc} \\ L_{qd}^{inc} & L_q^{inc} \end{bmatrix}, \quad (5)$$

$$\boldsymbol{L}_{\boldsymbol{dq,adj}}^{\boldsymbol{inc}} = \begin{bmatrix} L_{d,\mathrm{adj}}^{inc} & 0 \\ 0 & L_{q,\mathrm{adj}}^{inc} \end{bmatrix}, \quad (6)$$

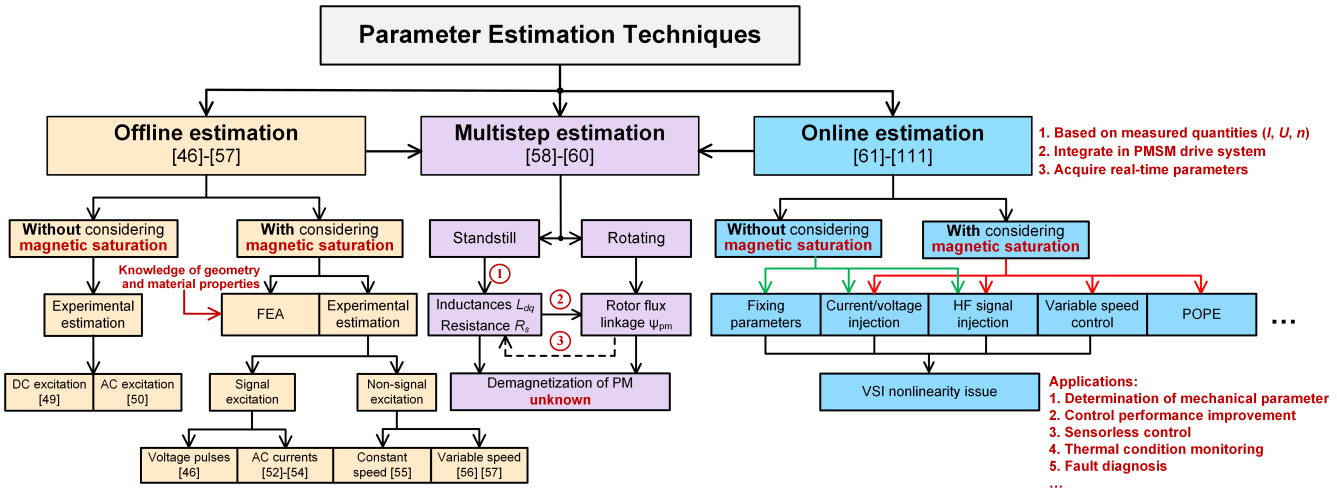

FIGURE 2. Overview of parameter estimation techniques.

where

$$L_{d,\mathrm{adj}}^{inc} = \frac{L_d^{inc}\Delta i_d + L_{dq}^{inc}\Delta i_q}{\Delta i_d}, \tag{7a}$$

$$L_{q,\mathrm{adj}}^{inc} = \frac{L_q^{inc}\Delta i_q + L_{qd}^{inc}\Delta i_d}{\Delta i_q}. \tag{7b}$$

Thus, the equivalent apparent inductances, L_d^a and L_q^a, can be calculated by [90]

$$L_d^a = \frac{\int L_{d,\mathrm{adj}}^{inc}(i_d)di_d}{i_d}, \tag{8a}$$

$$L_q^a = \frac{\int L_{q,\mathrm{adj}}^{inc}(i_q)di_q}{i_q}. \tag{8b}$$

It is worth mentioning that there is a third type of inductance definition [47], [48], which is often called energy inductance and is different from either apparent inductance or incremental inductance, although when the magnetic circuit is linear their values are the same. However, owing to space limitations, it will not be discussed in this paper.

In summary, the estimation of stator inductances can be grouped as:

1) Estimation of apparent and incremental inductances without [49], [50] and with [52]–[57] accounting for self- and cross-saturation effects.
2) The relationship between the incremental and apparent inductance can be approximated by (5)-(8).

B. BASIC PARAMETER ESTIMATION TECHNIQUES

The state-of-the-art offline/online parameter estimation techniques with/without accounting for magnetic saturation are briefly outlined, as shown in Fig. 2, and the estimation methods for stator inductances are summarized in Table 1.

The FEA is the most common offline method to estimate PMSM parameters but requires detailed knowledge of geometric and material information. It is widely reported that FEA can be used to calculate a rotor flux linkage map and incremental/apparent *dq*-axis inductances accounting for magnetic saturation and cross-coupling. However, sometimes FEA methods [47], [48] are limited since some material properties are unknown or not completely acquirable. Hence, offline experimental estimation methods have been extensively developed in the last few decades. Some existing methods are listed below.

1) Multiparameter estimation:
   a) DC step voltage excitation [49].
   b) DC-axis square voltage excitation [50].
2) Magnetic model estimation:
   a) Dq-axis voltage pulse injection [46].
   b) Fast Fourier transform (FFT) analysis [51].
   c) AC signal excitation [52]–[54].
   d) Estimation under constant speed [55].
   e) Estimation under variable speed [56], [57].

Firstly, according to the time constant at transient state, the step DC voltage excitation tests at standstill in [49] are used to predict apparent inductance, but it cannot determine the rotor flux linkage or accurately consider the magnetic saturation effect. In [50], *dq*-axis square voltages are supplied to estimate stator resistance, apparent inductances, rotor flux linkage and the initial rotor position. However, the magnetic saturation effect is also not taken into consideration.

Accounting for self- and cross-saturation effects, [51] estimates *dq*-axis flux linkages based on the measured *dq*-axis currents at constant rotor speed, and then, the *dq*-axis incremental inductances are calculated by the partial derivatives of *dq*-axis flux linkages with respect to currents. However, the variation of stator resistance due to the temperature effect is not considered. AC signal excitations are employed to estimate incremental [52] and apparent inductances [53], [54], respectively, where the DC bias point sets the magnetic operating point in [52], and induced voltages and internal load angles are measured in [53], [54]. To identify *dq*-axis flux linkages and incremental inductances, the voltage pulses are

TABLE 1. Comparison of stator inductance estimation methods.

Method	Reference	Incremental inductance			Apparent inductance			Magnetic saturation	Remark
		L_d^{inc}	L_q^{inc}	$L_{dq}^{inc}(L_{qd}^{inc})$	L_d	L_q	$L_{dq}(L_{qd})$		
Offline stator inductance estimation									
FEA	[47][48]	✓	✓	✓					Utilizing energy perturbation methods.
Experimental estimation	[49]				✓	✓		■	Time constant calculation.
	[50]				✓	✓		■	*Dq*-axis square voltage test.
	[53]				✓	✓		✓	Estimation based on induced voltages.
	[54]				✓	✓		✓	Estimation based on phasor diagram.
	[57]*				✓	✓		✓	Constant currents at variable speed control on the basis of steady-state equation.
	[46]*	✓	✓	✓				✓	Injection of voltage pulses at locked rotor.
	[51]*	✓	✓	✓				■	Inductances calculated by derivatives of flux linkages.
	[52]*	✓	✓	✓				✓	Injection of DC-biased AC at locked rotor.
Online stator inductance estimation									
Multistep estimation (steady-state)	[58][59][60]				✓	✓		■	PM demagnetization deteriorates accuracy.
d-axis signal injection (steady-state)	[61][62][63][70][73]				✓	✓		■	Both self- and cross-saturation effects are not considered.
	[74]				✓	✓		■	AC signal injection caused incremental inductances are ignored.
	[75][76][77]				✓	✓		Self-saturation	Cross-saturation is ignored.
Variable speed control (steady-state)	[80][81]				✓	✓		Self-saturation	Cross-saturation is ignored.
HF signal injection	[83]	✓	✓					Self-saturation	Cross-coupling is neglected.
	[84]	✓	✓					Self-saturation	Cross-coupling is neglected.
	[85]	✓	✓	✓				✓	Many empirical coefficients are required.
	[86]	✓	✓	✓				✓	Special algorithm is used to realize online computation.
	[89]	✓	✓	✓				✓	Rotating and pulsating HF signal injections.
	[90]	✓	✓	✓	✓	✓	✓	✓	HF apparent inductances are estimated by using curve fitting.
Zero-voltage vector	[91][92]				✓	✓		■	Inductances are fixed to nominal values.

"✓": Considered; "■": not reported.
Based on estimated *dq*-axis flux linkages, [46]*, [51]* and [52]* calculate incremental inductances (3), while [57]* calculates apparent inductances (4).

applied to *d*-axis and *q*-axis in turn while the other axis current remains constant [46]. However, the integration of applied voltage is sensitive to the DC offsets. In [55]–[57], magnetic models are estimated based on the FOC schemes at constant [55] and at variable speed [56], [57]. More specifically, [55] requires an additional voltage measurement circuit. The variations of stator resistance and VSI caused distorted voltage is determined at standstill [56]. The *dq*-axis flux-linkage map is modelled as second-order polynomials under variable speed control [57]. It should be mentioned that the estimated *dq*-axis flux linkages in [46], [51], [52] and [57] can derive both incremental and apparent inductances based on (3)-(4). However, the values of two type inductances may be different due to magnetic saturation, and the above papers select either incremental or apparent inductance. In addition to the direct calculation by means of inductance definitions, the apparent inductances can also be estimated by utilizing the time constant of armature winding circuit [49], as well as the analysis of a phasor diagram [54].

Secondly, the multistep estimation utilizes the acquirable parameters, e.g. stator resistance and distorted voltage drop, at standstill, and then, the rotor flux linkage and the stator apparent inductances can be estimated in the operating state [58]–[60]. Nevertheless, it cannot accurately track online parameter variations due to neglecting the magnet temperature rise and the core loss, which will be presented in Section IV A in detail.

Thirdly, without relying on the nominal values/offline measurement, the online estimation methods are conducted during the operation based on the available input and output

measured quantities, i.e. current (I), voltage (U) and rotor speed (n). On the one hand, with temperature increasing, the value of stator resistance increases while the value of rotor flux linkage decreases. Thus, these real-time estimated temperature-dependent parameters can monitor the thermal states [65], [66], thereby, preventing the damage of winding insulation and PM demagnetization. It is particularly beneficial to the estimation of temperature in PMs on the rotor where direct temperature measurement is difficult. On the other hand, there are some new developments in the current research of observers, for instance, in [8], the peak energy spectrum is creatively introduced into the flux linkage observer, while a bearing fault diagnosis based on a full-order observer is firstly proposed and applied, which has a groundbreaking significance, and this research direction is worthy of attention. The abrupt changes in dq-axis inductances and stator resistance can also be used to diagnose the inter-turn short-circuit (ITSC) [67]–[71].

Although the online parameter estimation techniques incorporate high levels of computational efficiency, with the improvement of the computing capability of the processor, some AI-based algorithms have been applied to online parameter estimations to monitor thermal states of winding and PM, whose temperatures vary slowly, e.g. [70]–[81]. Most online methods are concerned with the apparent inductance estimation since the terms of time derivation of dq-axis flux linkages are cancelled in the steady-state equation [70]–[92]. However, the injected AC signals [74] will induce non-negligible incremental inductances, which have not been considered in the PMSM model (1)-(2). Meanwhile, due to the limited rank of the reference model, most papers do not take into account of the effect of cross-saturation. HF incremental inductances are also important for high frequency signal injection based sensorless rotor position estimation, particularly at zero and low speed, which has been investigated in [83]–[90]. The main online modelling techniques, including HF signal injection, will be illustrated in Section IV in greater detail. However, there are still some general issues in the parameter estimation, e.g. rank-deficient problem, VSI nonlinearity, as well as the influence of signal injection, which must be addressed first.

III. BASIS OF PMSM AND GENERAL ISSUES OF PARAMETER ESTIMATION

In the last few decades, numerous PMSM topologies have been developed [1], with the common configurations being shown in Fig. 3. The surface-mounted PMSM (SPMSM), Fig. 3 (a), has a simple construction and higher power density, but it can only produce PM torque due to non-saliency and the magnets are directly exposed to the armature reaction field, and consequently, the stator inductances are relatively low and almost equal in dq-axes. In comparison, the interior PMSM (IPMSM), Fig. 3 (b), is constructed with magnets embedded in the rotor core, and has a high saliency ratio, i.e. q-axis inductance $>$ d-axis inductance. Thus, these machines are able to utilize the reluctance torque.

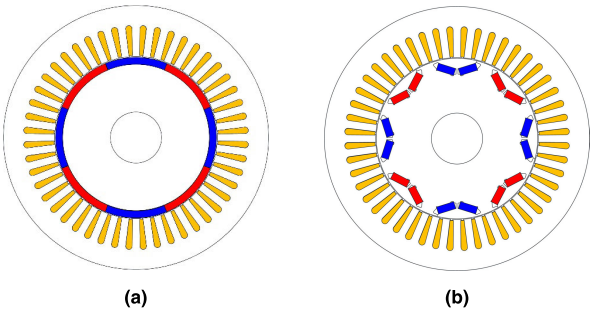

FIGURE 3. Common configurations of PMSMs. (a) SPMSM. (b) IPMSM.

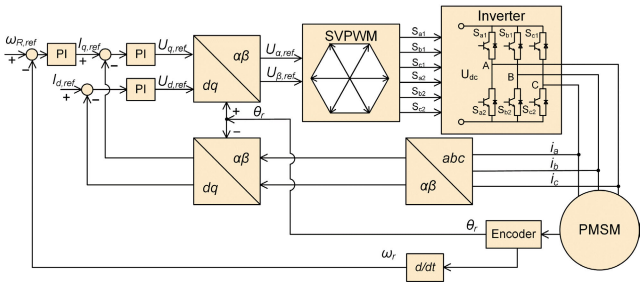

FIGURE 4. Scheme of FOC system.

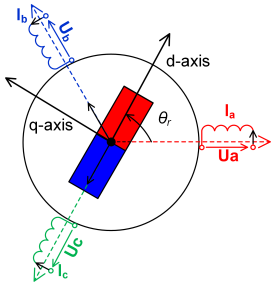

FIGURE 5. Representation of rotating dq-axis frame.

Fig. 4 shows the scheme of the most popular FOC system, where the currents are represented by a space vector in the dq-axis rotating frame, Fig. 5. The Park transformation from three-phase currents to dq-axis currents is expressed as

$$\begin{bmatrix} i_d \\ i_q \end{bmatrix} = \frac{2}{3}\boldsymbol{T_{abc}} \begin{bmatrix} i_a \\ i_b \\ i_c \end{bmatrix},$$
$$\boldsymbol{T_{abc}} = \begin{bmatrix} \cos(\theta_r) & \cos\left(\theta_r - \frac{2\pi}{3}\right) & \cos\left(\theta_r + \frac{2\pi}{3}\right) \\ -\sin(\theta_r) & -\sin\left(\theta_r - \frac{2\pi}{3}\right) & -\sin\left(\theta_r + \frac{2\pi}{3}\right) \end{bmatrix}, \tag{9}$$

where θ_r is the rotor angular position.

The PMSM model in the dq-axis frame is expressed in (1)-(2), and the electromagnetic torque is

$$T_e = \frac{3}{2}p\left[\psi_{pm} i_q + \left(L_d - L_q\right) i_d i_q\right], \tag{10}$$

where p is the number of pole-pairs. For non-salient PMSM, it is assumed that $L_d = L_q = L_s$.

The mechanical equation is described as

$$J\frac{d\omega_r}{dt} = p\left(T_e - T_L - \frac{B}{p}\omega_r\right), \tag{11}$$

where J is the rotor inertia. T_L is the load torque. B is the friction coefficient.

Based on the above electrical and mechanical equations, one or more electrical and mechanical parameters can be estimated with aid of the measured basic electrical quantities, i.e. current, voltage, rotor speed. However, some critical issues still need to be emphasised, i.e. rank-deficient and ill-condition problems, inverter nonlinearity, as well as the influence of invasive signal, as illustrated in Fig. 6 and described below.

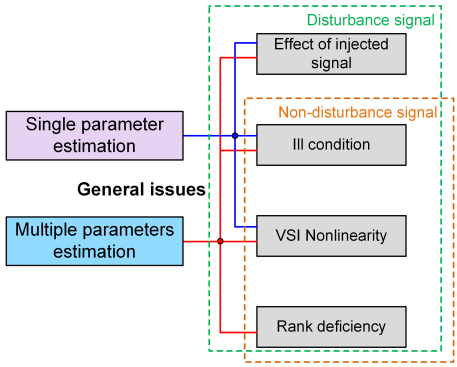

FIGURE 6. General issues in single/multiple parameter estimation.

A. RANK-DEFICIENT PROBLEM

The rank-deficient problem in PMSMs is systematically investigated in [61], which reveals that the accurate parameter estimation relies on the full-rank reference/variable system. As can be seen from (1)-(2), the rank of the electrical model of the PMSM is two, and thus, only two parameters can be estimated simultaneously. If the number of unknown parameters is more than the rank of the system, the estimated results may not be converged to the correct values [95], [96].

Taking results in [61] as an example, on the basis of a nonsalient-pole PMSM, the nominal values of ψ_{pm}, R_s, and L_s are 77.6 mWb, 0.373 Ω, and 3.24 mH, respectively. By utilizing the ANN estimator and one set of the electrical equation, if the initial values are set far from the nominal values, it will lead to significant estimation errors for all three parameters, as shown in Fig. 7.

In order to mitigate the ill-convergence problem and realize the simultaneous estimation of multiple parameters, several approaches have been proposed and summarised as:

1) Injection signals at standstill [49]–[52].
2) Fixing one or more parameters [95]–[109].
3) Utilizing different states at standstill and operation [58]–[60].
4) With aid of additional devices, i.e. thermal sensors, power/torque meters [53], [65], [110].
5) Injecting disturbance signals, [61]–[63], [70]–[94].

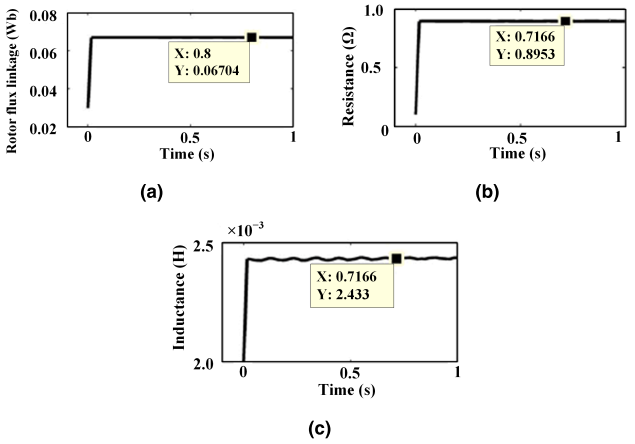

FIGURE 7. Examples of issues under rank-deficient condition [61]. (a) Estimated rotor flux linkage. (b) Estimated stator resistance. (c) Estimated inductance. Nominal values of rotor flux linkage, stator resistance and inductance are 77.6 mWb, 0.373 Ω, and 3.24 mH.

Several methods [49]–[52] have been proposed to estimate electrical parameters for PMSMs at standstill, or in the case of a locked rotor, which can eliminate the influence of rotor flux linkage. The injected signals include DC step voltage [49], AC signals [50]–[52], etc. However, the offline estimation cannot track the variation of parameters, especially for some parameters, which are heavily influenced by operating conditions.

Secondly, to ensure full-rank, a simple method is to fix one or more parameters in the parameter estimation. For instance, R_s, L_d, and L_q are estimated in [98] by using RLS while the other parameters are fixed to the nominal values to build a full-rank reference/variable model. In [100], EKF is used to estimate ψ_{pm}, which relies on a prior knowledge of the nominal values of R_s, L_d, and L_q. In [101], MRAS and EKF estimators are used to estimate speed/position and ψ_{pm} separately, while R_s, L_d and L_q are set as the nominal values. To ease the considerable computational burden due to inverse matrix computation (A.9), the full-order EKF is divided into two independent reduced-order EKFs in [102] to estimate R_s, L_d, L_q and ψ_{pm} based on the assumption of $dR_s/dt = 0$ and $d\psi_{pm}/dt = 0$ alternately. A three-order EKF is developed in [104] to estimate ψ_{pm} while the variations of L_d and L_q are ignored. In [109], R_s and ψ_{pm} are estimated at low and high speeds, respectively. However, these two parameters cannot be estimated simultaneously, and the rotor speed needs to be changed for estimation. However, it is demonstrated that if R_s and ψ_{pm} are not estimated simultaneously but separately, the two estimated parameters may be converged to the wrong values due to the mismatch of the actual and nominal parameter values under different load conditions [61]. The detailed descriptions of RLS and EKF algorithms are given in Appendices A and B, respectively.

Thirdly, the two-step and three-step estimation procedures are proposed in [58]–[60] to estimate electrical parameters at standstill and operating state. However, the variation of rotor flux linkage due to temperature dependency strongly affects

the estimation accuracy, which will be illustrated in detail in Section IV.

Fourth, the power meter [53], thermal couples [65], as well as thermal imager [110] are used to provide extra machine information. However, these methods require additional devices or constructional changes and suffer from the risk of sensor/device failure, which is not appropriate to low-cost industrial applications.

Finally, from the other perspective, the full-rank reference system can also be modelled by introducing additional disturbance signals to change the PMSM states, i.e.

1) Current/voltage injection [61]–[63], [70]–[79].
2) Rotor position offsets [35], [66], [81].
3) Variable rotor speed [80], [81].
4) HF signal injection [82]–[90].
5) Zero-voltage vector injection [91], [92].
6) Speed harmonics [93], [94], etc.

Therefore, the values of nominal parameters are usually no longer required and the multiple parameters can be possibly estimated simultaneously. The detailed overview will be presented in Section IV.

B. ILL-CONDITION PROBLEM

The uncertainties of the PMSM model and measurement noises may also deteriorate the performances of parameter estimation and result in decreased process reproducibility, which is called ill-condition mathematically [111], [112]. The ill condition implies that the estimated parameters are very sensitive to perturbations in the input and output data due to sensor noise and the computation process.

For example, considering the following systems:

$$\begin{cases} x + y = 2, \\ x + 1.001y = 2. \end{cases} \qquad \begin{cases} x + y = 2, \\ x + 1.001y = 2.001. \end{cases} \tag{12}$$

The left system has solution $x = 2$, $y = 0$ while the right system has the other solution $x = 1, y = 1$. A small change in the inputs or in the constant coefficients will result in a large change in the solution, and it will lead to misestimation.

The condition number $cond(A)$ is applied to judge how sensitive it is to errors in the input and defined as

$$cond(A)_v = \left\| A^{-1} \right\|_v \|A\|_v , \tag{13}$$

where "v" is the operator norm of matrix A. The system equations are called ill-conditioned if $cond(A)_v$ is much larger than one, otherwise, they are called well-conditioned.

C. INVERTER NONLINEARITY

Since the direct measurement of the terminal voltage is difficult, reference voltages are often employed for the estimation. Nevertheless, the nonlinearity of VSI will introduce distortion to both the reference and real voltages. Consequently, it will lead to estimation errors due to ill-condition problem.

As detailed in [113], [114], the correlations between the terminal voltages $u_{d,q}$ and the reference voltages $u^*_{d,q}$ are shown as

$$\begin{cases} u^*_d = u_d + D_d V_{dead} \\ u^*_q = u_q + D_q V_{dead} \end{cases}, \tag{14}$$

where $D_d V_{dead}$ and $D_q V_{dead}$ are the distorted voltage terms in d- and q-axes, which are expressed as

$$V_{dead} = \frac{1}{3}\left(\frac{2V_{dc}(t_d + t_{on} - t_{off})}{Ts} + V_{ce} + V_{d0} \right), \tag{15}$$

$$\begin{bmatrix} D_d \\ D_q \end{bmatrix} = \begin{bmatrix} \sin\theta_e & \sin(\theta_e - 2/3\pi) & \sin(\theta_e + 2/3\pi) \\ \cos\theta_e & \cos(\theta_e - 2/3\pi) & \cos(\theta_e - 2/3\pi) \end{bmatrix} \times \begin{bmatrix} \mathrm{sgn}(i_a) \\ \mathrm{sgn}(i_b) \\ \mathrm{sgn}(i_c) \end{bmatrix}, \tag{16}$$

where V_{dc}, V_{ce}, and V_{d0} are the DC bus voltage, the threshold voltages of the active switch and the freewheeling diode, respectively. θ_e is the rotor position. t_d, t_{on} and t_{off} are the pulsewidth modulation (PWM) dead-time, turn-on and turn-off time delays of the switch, respectively.

The sign function (sgn) is expressed as

$$\mathrm{sgn}(i) = \begin{cases} 1, & i \geq 0, \\ -1, & i < 0. \end{cases} \tag{17}$$

However, theoretical voltage compensation cannot be 100% accurate due to uncertain VSI parameters and measurement errors. In [62], the estimation error due to nonideal compensation is analysed and minimized by using an error analysis, where the nonideal voltage measurement is compensated as:

1) Read the zero-shift voltage V_{offset} of the analog-to-digital converter (ADC) at zero speed with V_{dc}= 0;
2) The actual DC bus voltage is compensated by subtracting V_{offset} from the measured bus voltage V_m;
3) The compensation voltage V_{com} is calculated;
4) The computed V_{offset} and V_{com} will be employed for compensating the dq-axis voltages measured from the output of the PI regulators.

It has been revealed in [64] that the VSI nonlinearity compensation has a significant influence on the estimation of R_s and ψ_{pm} at low speed, while, at high speed, it only affects the estimation accuracy of R_s. Under $i_d = 0$ control, the influence of VSI nonlinearity on the estimation of L_q is negligible, while L_q is sensitive to the DC bus voltage drop due to load variation and zero shift in the amplifier.

Fig. 8 shows the estimated stator resistance and rotor flux linkage with and without considering the influence of nonideal voltage measurement at $\omega = 157$ rad/s in [64], where the nominal values of R_s and ψ_{pm} are 0.33 Ω and 0.0776 Wb. Compared with Figs. 8 (a)-(b), Fig. 8 (c) shows much better results, which are close to the nominal values.

Due to the significance of VSI nonlinearity, an ANN estimator in [65] is employed to estimate the distorted voltage V_{dead} (14)-(17) and ψ_{pm} with the aid of thermocouples inserted in the stator winding. The compensation method is applied to the FOC system in Fig. 9. Fig. 10 shows the dq-axis

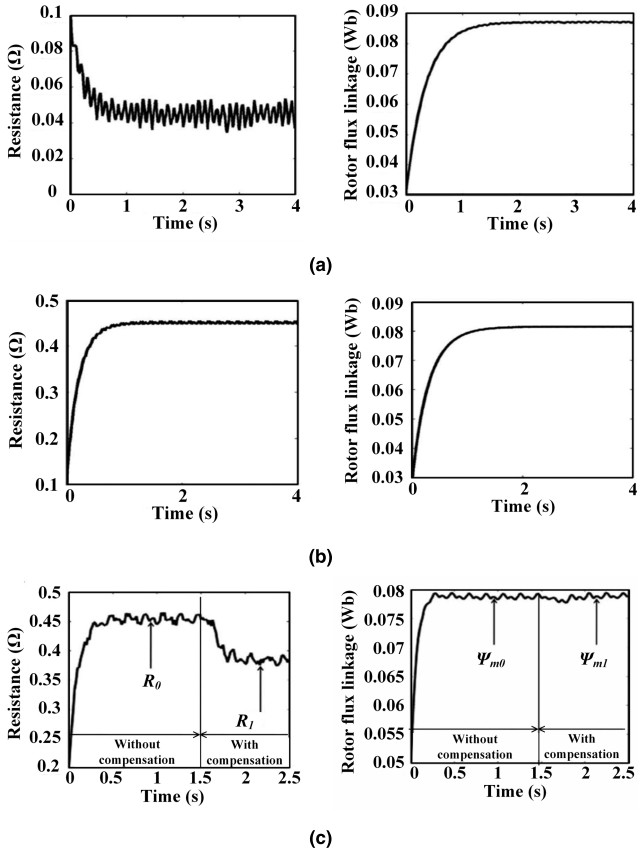

FIGURE 8. Estimated stator resistance and rotor flux linkage [64]. (a) Without considering the voltage nonidealities. (b) Considering the measurement of DC bus voltage variation and the DC offset due to zero shift. (c) Considering the measurement of DC bus voltage variation, the dc offset due to zero shift, and the VSI nonlinearity compensation.

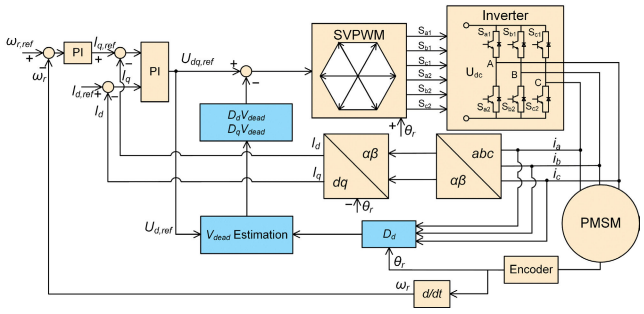

FIGURE 9. Compensation of VSI nonlinearity based on FOC system [65].

currents with and without considering voltage compensation at 300 r/min based on the experimental results. Obviously, the online tuning process of VSI nonlinearity will significantly reduce the fifth and seventh current harmonics.

D. INFLUENCE OF SIGNAL INJECTION

The convergence speed and excitation duration have been widely used to analyse the stability properties of different parameter estimation algorithms [115]. The excitation duration of the input signals should take into account the

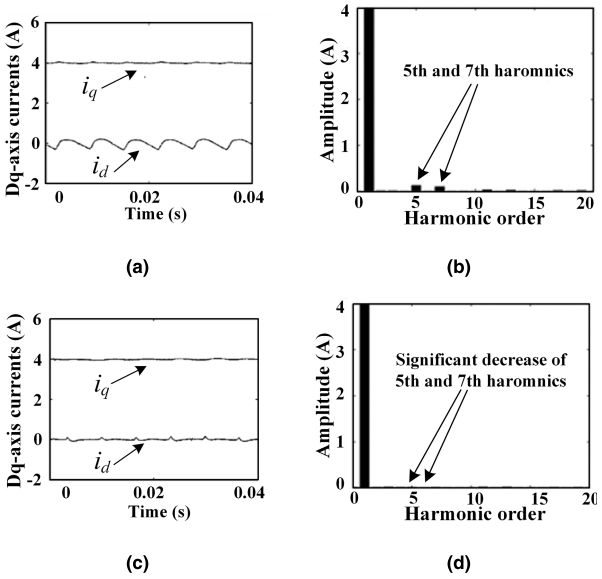

FIGURE 10. Measured dq-axis currents and spectra [65]. (a)-(b) Without proposed compensation. (c)-(d) With proposed compensation.

convergence speed of the applied algorithms. To build the full-rank reference model, the injected current excitations will affect the cross- and self-saturation of stator inductances and introduce additional reluctance torque for interior PMSMs and torque ripples for surface-mounted PMSMs.

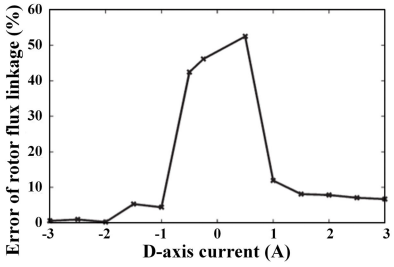

FIGURE 11. Error analysis of estimation error of rotor flux linkage [61].

In [61], since the variations of L_d, L_q and ψ_{pm} due to magnetic saturation with the injected d-axis current is neglected in the parameter estimation, the estimation errors are analysed and minimized by increasing the amplitude of the injected negative d-axis current, as shown in Fig. 11. Moreover, q-axis current compensation [76] and window functions [78], [79] are presented to restrain the current injection caused torque ripple and the excitation of resonances, respectively.

IV. EXISTING MODELING TECHNIQUES FOR ONLINE PARAMETER ESTIMATION

Generally, the online parameter estimation process is integrated on the basis of the PMSM drive system under sensored and sensorless control. Both the electrical and mechanical parameters can be estimated by utilizing the various estimation algorithms and the measured quantities. The schematic diagram of online parameter estimation is shown in Fig. 12,

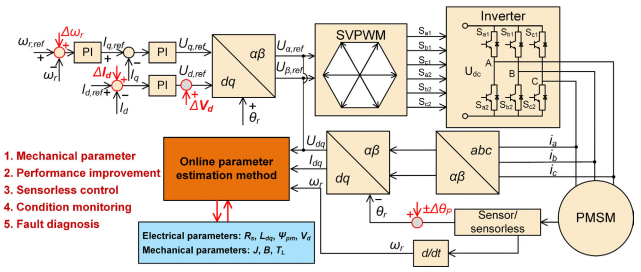

FIGURE 12. Schematic diagram of online parameter estimation.

where $\Delta\omega_r$, ΔI_d, ΔV_d, and $\Delta\pm\theta_p$ are variables of rotor speed, injected d-axis current and voltage, as well as the position offsets. Sometimes the knowledge of some electrical parameters is also required [35], [65], [80] and [81].

A reliable estimation model is the crucial precondition of online parameter estimation techniques. If the estimation model is built appropriately, it is not sensitive to the employed estimation algorithms. The widely used modelling techniques are overviewed below.

A. MULTISTEP ESTIMATION

As aforementioned, the rank-deficient problem restricts the multi-parameter estimation. To mitigate this issue, the simplest modelling techniques are multistep estimations, i.e. the two-step [58] and the three-step estimations [59].

It has been demonstrated in [58] that R_s and ψ_{pm} cannot be estimated simultaneously under sensorless control. The two-step estimation is designed as follows.

1) At the first step, ψ_{pm} is fixed as nominal value to estimate R_s.
2) At the second step, R_s is fixed as nominal value to estimate ψ_{pm}.

Overall, the two-step estimation can be easily implemented, but the estimation accuracy will deteriorate due to variation of parameters, especially the decrease of ψ_{pm} at high temperature. Meanwhile, since L_s is set to its nominal value, the influence of magnetic saturation variation cannot be considered.

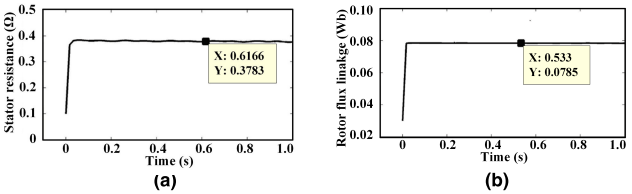

FIGURE 13. Estimated stator resistance and rotor flux linkage at room temperature under two-step estimation [116]. (a) Stator resistance. (b) Rotor flux linkage.

Under $i_d = 0$ control, by utilizing an MRAS estimator, the experimentally estimated R_s and ψ_{pm} at room temperature and after heating are shown in Figs. 13-14. The description of MRAS is given in Appendix C. As can be seen, the estimated values of R_s and ψ_{pm} at room temperature are close

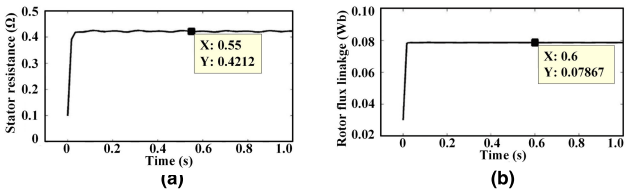

FIGURE 14. Estimated stator resistance and rotor flux linkage after heating under two-step estimation [116]. (a) Stator resistance. (b) Rotor flux linkage.

to the nominal values of 0.373Ω and 0.0776Wb. However, the estimated stator resistance of 0.42Ω is smaller than the measured value of 0.45Ω, and the estimated rotor flux linkage increases to 0.0786 Wb, which is opposite to the physical properties of NdFeB magnet since as the temperature increases the PM flux linkage should be reduced.

The procedure of three-step estimation [59] is implemented as follows.

1) At the first step, R_s and V_{dead} are estimated by signal injection at standstill.
2) At the second step, ψ_{pm}, L_d and L_q are estimated at the operating state by fixing the estimated values at the first step.
3) At the third step, the variations of R_s, L_d and L_q are estimated online by fixing ψ_{pm} at the second step.

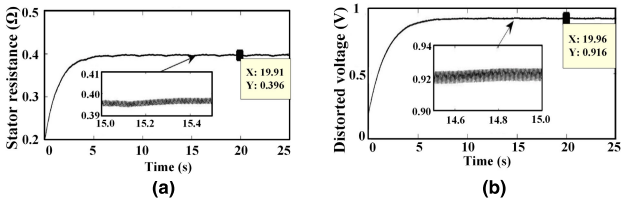

FIGURE 15. Estimated stator resistance and distorted voltage at standstill under three-step estimation [116]. (a) Stator resistance. (b) Distorted voltage.

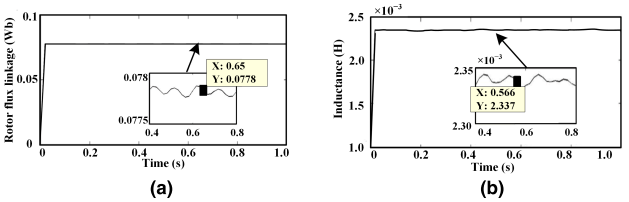

FIGURE 16. Estimated stator inductance and rotor flux linkage at operating state under three-step estimation [116]. (a) Rotor flux linkage. (b) Stator inductance.

The accuracy of three-step estimation is also affected by the variation of ψ_{pm}. The three-step estimation is also verified experimentally and shown in Figs. 15-17. Figs. 15 and 16 show the estimated R_s and V_{dead} by injecting d-axis current at standstill, as well as the estimated ψ_{pm} and L_s at operating state.

After 30 mins and 60 mins operation, Fig. 17, the measured R_s are 0.41Ω and 0.42 Ω, respectively, which are

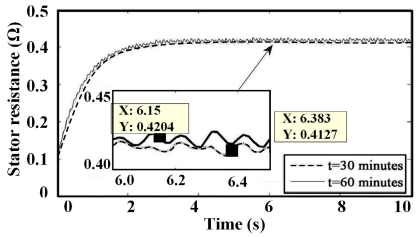

FIGURE 17. Estimated stator resistance after heating under three-step estimation [116].

slightly larger than the measured values of 0.40 Ω and 0.41Ω. The estimation errors can be attributed to several factors, i.e. imperfect compensation of VSI, measurement error, as well as decreasing variation of ψ_{pm} with temperature-rise.

B. CURRENT/VOLTAGE INJECTION

In the cases without adding extra hardware devices, d-axis current/voltage injection is widely used to change the state of PMSM, which can build a full-rank reference model to estimate multiple parameters. The injected signal can also be in different forms.

1) Alternating sinusoidal currents [74].
2) One/multiple level negative d-axis current pulses [61]–[63], [70], [73], and [75].
3) DC-component current [76].
4) Harmonic voltage injection [77].

Based on the full rank reference model, various estimation algorithms have been employed to realize multiple parameter estimation, i.e. RLS [75], [76], ANN [61], [62], EAs [63], [70], [73]. For instance, L_d, L_q, R_s, ψ_{pm} and V_{dead} are estimated by seven individual objective functions in [63] by utilizing self-learning PSO by injecting a short period of $i_d \neq 0$. Similarly, a coevolutionary PSO is designed in [73] to estimate L_d, L_q, R_s and ψ_{pm}, where the graphic processing unit (GPU) is used to accelerate computational efficiency. The PSO algorithm is introduced in Appendix D in detail. In [74], both R_s and back-electromotive-force (EMF) coefficient are estimated by superimposing a small AC component on the d- axis current under steady-state sensorless operation, while L_d and L_q are assumed to be known in a prior.

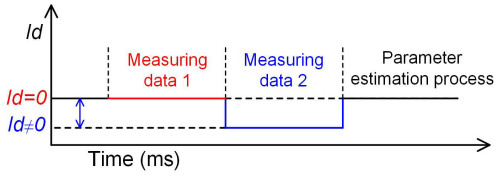

FIGURE 18. Measurement process based on d-axis current injection.

Under $i_d = 0$ control, the measurement process based on d-axis is shown in Fig. 18, where the subscripts "0" and "1" denote the measured data when $i_d = 0$ and $i_d \neq 0$, respectively. Under the assumption that the magnetic saturation is ignored, the ANN estimator is used to estimate R_s, ψ_{pm}, and L_s simultaneously in [61]. The estimation results are shown in

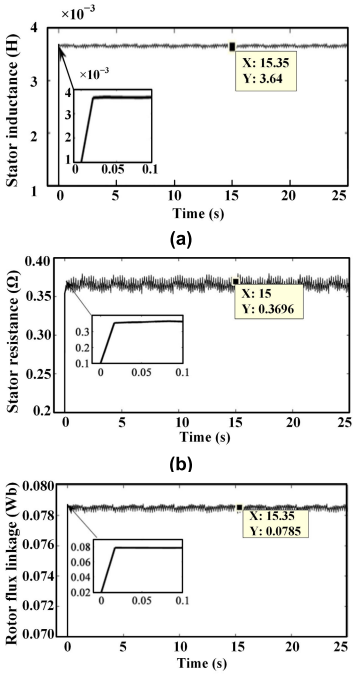

FIGURE 19. ANN estimated parameters based on d-axis current injection [61]. (a). Stator inductance. (b) Stator resistance. (c) Rotor flux linkage.

Fig. 19, where the measured values are 0.373 Ω, 87.4 mWb, and 3.24 mH. The injected d-axis current equals −2A and lasts 50 ms. The modelling of ANN estimator can be found in Appendix E.

Accounting for the cross- and self- magnetic saturation of dq-axis inductances, the stator inductances are no longer constant and can be expressed as follows:

$$L_d = f_d\left(i_d, i_q\right), \quad L_q = f_q(i_d, i_q). \tag{18}$$

For simplicity, the linear correlation (19) is proposed to describe the saturation effect during the current injection in [75], [76], where α_d, α_q and β_d, β_q are the cross- and self-saturation constants. However, the introduced saturation coefficients will increase the number of unknown parameters, and thus, the estimation process must contain sufficient signal injections, e.g. multi-level, DC/AC component based current injections, etc.

$$L_d = l_{d0} - \beta_d i_d - \alpha_q i_q, \quad L_q = l_{q0} - \beta_q i_q - \alpha_d i_d. \tag{19}$$

C. POSITION-OFFSET-BASED ESTIMATION

A position-offset-based parameter estimation (POPE) is proposed in [66], where ψ_{pm} can be estimated based on the transient addition of small positive and negative position offsets. In the proposed method, the influences of VSI nonlinearity and magnetic saturation are eliminated. With the aid of estimated ψ_{pm}, R_s can be determined sequentially. The measurement process of POPE is shown in Fig. 20, where θ_p and θ_n are positive and negative position offsets.

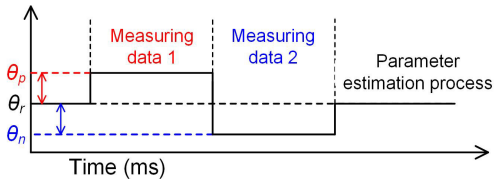

FIGURE 20. Parameter estimation process based on position offsets.

The estimation model of POPE is expressed as

$$\begin{aligned} u_{d1}^* - D_d V_{dead} &= R_s i_d - \omega \left(L_q i_q + \psi_{pm} \sin\left(\theta_r + \theta_p\right) \right), \\ u_{d2}^* - D_d V_{dead} &= R_s i_d - \omega \left(L_q i_q + \psi_{pm} \sin(\theta_r + \theta_n) \right). \end{aligned} \tag{20}$$

Thus, ψ_{pm} can be obtained by

$$\omega \psi_{pm} \cos(\theta_r) = \frac{u_{d1}^* - u_{d2}^*}{2\sin(\theta_n)}. \tag{21}$$

Under $i_d = 0$ control, the stator resistance is obtained as

$$R_s = \frac{u_q^* - D_q V_{dead} - \frac{u_{d1}^* - u_{d2}^*}{2\sin(\theta_n)}}{i_q}. \tag{22}$$

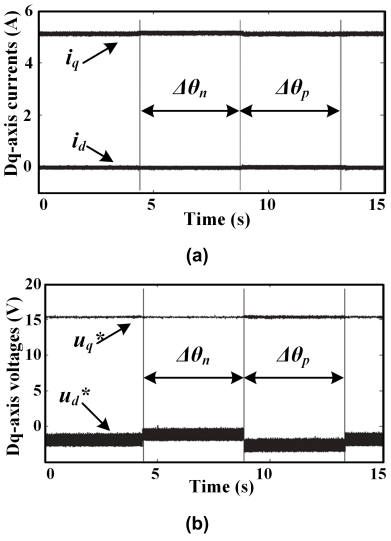

FIGURE 21. Measured dq-axis voltages and currents based on POPE [66]. (a) Currents. (b) Voltages.

By utilizing the ANN estimator in [66], the dq-axis voltages and currents at 300 r/min with $\theta_p = 10\theta_u$, and the estimated R_s and ψ_{pm} are shown in Figs. 21 and 22, respectively, where θ_u is the unit electrical angle. Obviously, the position offsets have a significant effect on the d-axis voltage. The estimated parameters are presented in Fig. 22, where $i_d = 0$, $i_q = 4$A at 300 r/min. In comparison to the nominal values of 70.7 mWb and 0.33 Ω, the estimated values agree well. The POPE technique can be further applied to estimate mechanical parameters after accurately acquiring torque constant [35], which will be introduced in Section VI A.

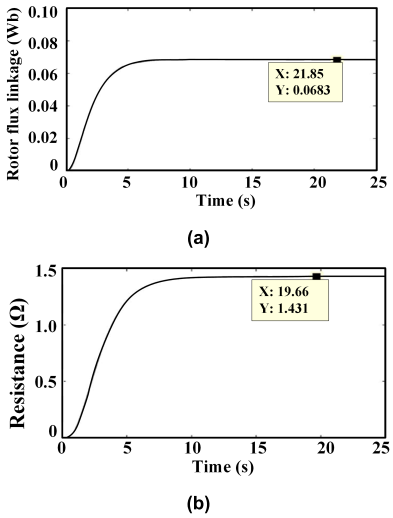

FIGURE 22. Estimated parameters based on POPE [66]. (a) Stator resistance. (b) Rotor flux linkage.

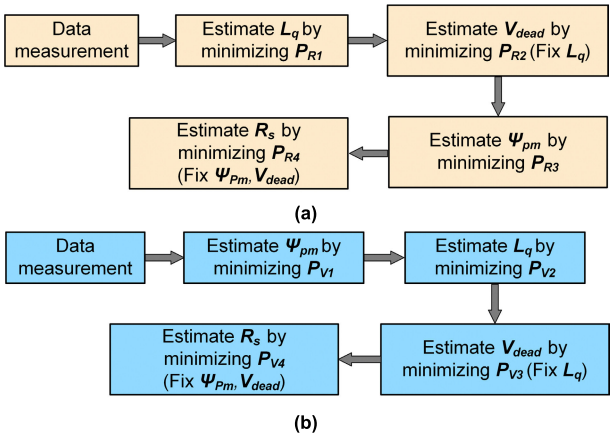

FIGURE 23. Procedures of QGA based parameter estimation. (a) Variable speed based estimation [80]. (b) Rotor position-offset based estimation [81].

D. ESTIMATION UNDER VARIABLE SPEED CONTROL

A full rank reference model under variable speed control is proposed in [80], [81] and the estimation procedures are given in Fig. 23. Since the dq-axis currents remain constant and only the rotor speed is changed, the estimation strategy under variable speed control is preferred to take into account the cross- and self-saturation effects. Due to large thermal time constants of both the winding and PM, a quantum genetic algorithm (QGA) is used under the variable speed control. The detailed description of GA can be found in Appendix F.

Firstly, the steady-state dq-axis PMSM model (14) under $i_d = 0$ control can be further simplified as

$$\begin{cases} u_d^* = -\omega_r \hat{L}_q i_q + D_d \hat{V}_{dead} \\ u_q^* = \hat{R}_s i_q + \omega_r \hat{\psi}_{pm} + D_q \hat{V}_{dead} \end{cases} \tag{23}$$

Since $D_d V_{dead}$ is a zero-mean distorted voltage under $i_d = 0$ control, and thus, it will not influence the estimation of L_q. Afterwards, the other parameters, i.e. V_{dead}, ψ_{pm}, and R_s,

can be estimated subsequently based on the individual cost functions $\boldsymbol{P_{Vi}}$.

The cost functions $\boldsymbol{P_{V1}} - \boldsymbol{P_{V4}}$ in [80] are expressed as

$$\boldsymbol{P}_{\boldsymbol{V1},\hat{L}_q,\hat{V}_{dead}} = \sum_{k=1}^{n} \left(K_u \left| u^*_{d,k} + \hat{L}_q \omega_{r,k} i_{q,k} - D_{d,k} \hat{V}_{dead} \right| \right), \quad (24)$$

$$\boldsymbol{P}_{\boldsymbol{V2},\hat{V}_{dead}} = \sum_{k=1}^{n} \left(K_v \left| u^*_{d,k} + L_q \omega_{r,k} i_{q,k} - D_d \hat{V}_{dead} \right| \right), \quad (25)$$

$$\boldsymbol{P}_{\boldsymbol{V3},\hat{\psi}_{pm}} = \sum_{k=1}^{n} \left(K_m \left| u^*_{q,k-(k+0.5n)} - \hat{\psi}_{pm} \omega_{r,k-(k+0.5n)} \right| \right), \quad (26)$$

$$\boldsymbol{P}_{\boldsymbol{V4},\hat{R}_s} = \sum_{k=1}^{n} \left(K_w \left| u^*_{q,k} - \hat{R}_s i_{q,k} - \psi_{pm} \omega_{r,k} - D_q V_{dead} \right| \right), \quad (27)$$

where subscript k denotes the sampling index; n is the length of the measured data; $K_{u,u,m,w}$ are the gains of cost function. Finally, L_d is estimated under the assumption that the transient load torque with/without small DC offset is constant.

In addition, similar to [80], POPE is further applied to estimate ψ_{pm} in [81], then the rest parameters, i.e. R_s, L_q and V_{dead}, are estimated from the measured data without the addition of position offset. The above proposed two parameter estimation procedures are applied to an IPMSM, in which the nominal values of ψ_{pm}, L_q and R_s are 236 mWb, 58.5 mH, and 6.0 Ω. The estimated values are shown in Figs. 24 and 25.

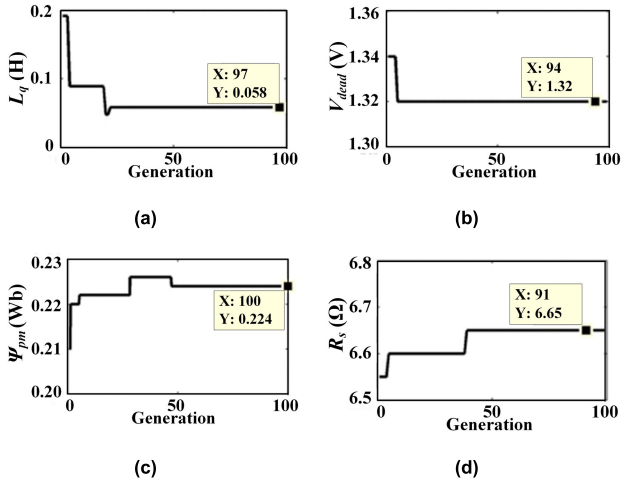

FIGURE 24. QGA estimated parameters under variable speed control [80]. (a) q-axis inductance L_q. (b) Distorted voltage V_{dead}. (c) Rotor flux linkage Ψ_{pm}. (d) Stator resistance R_s.

It is also worthwhile mentioning that the conventional cost function (28) is designed by minimizing the absolute errors of the measured currents, which has been widely used in existing PSO based parameter estimation PSO.

$$J = \sum_{k=1}^{n} \left(K_d \left| i_d(k) - \hat{i}_d(k) \right| + K_q \left| i_q(k) - \hat{i}_q(k) \right| \right), \quad (28)$$

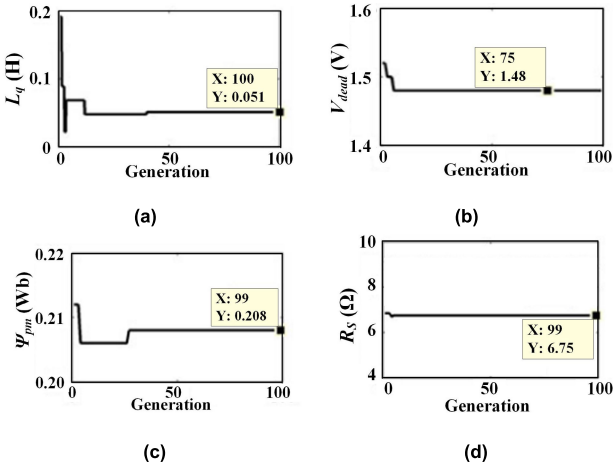

FIGURE 25. QGA estimated parameters based on POPE under variable speed control [81]. (a) q-axis inductance L_q. (b) Distorted voltage V_{dead}. (c) Rotor flux linkage Ψ_{pm}. (d) Stator resistance R_s.

where K_d and K_q are the weighting factors. i_d, $\hat{i}_d$, i_q and $\hat{i}_q$ are the measured and predicted dq-axis currents, respectively. In addition to the rank-deficient problem, the conventional cost function also tends to suffer from the VSI nonlinearity.

E. HIGH FREQUENCY SIGNAL INJECTION

The injection techniques of HF carrier signals have been widely studied as a means for sensorless control. Moreover, it can also be used to the PM temperature estimation, online inductance estimation, as well as torque estimation [83]–[90]. In [82], [83], HF signal injection methods are proposed to estimate the magnet temperature based on its correlation with the HF stator resistance or inductance. The HF signal injection-based estimation model is expressed as

$$\begin{bmatrix} v^r_{d\text{hf}} \\ v^r_{q\text{hf}} \end{bmatrix} = \begin{bmatrix} R_{d\text{hf}} & 0 \\ 0 & R_{q\text{hf}} \end{bmatrix} \begin{bmatrix} i^r_{d\text{hf}} \\ i^r_{q\text{hf}} \end{bmatrix} + \rho \begin{bmatrix} L_{d\text{hf}} & 0 \\ 0 & L_{q\text{hf}} \end{bmatrix} \begin{bmatrix} i^r_{d\text{hf}} \\ i^r_{q\text{hf}} \end{bmatrix} + \begin{bmatrix} 0 & -\omega_r L_{q\text{hf}} \\ \omega_r L_{d\text{hf}} & 0 \end{bmatrix} \begin{bmatrix} i^r_{d\text{hf}} \\ i^r_{q\text{hf}} \end{bmatrix}, \quad (29)$$

where $v^r_{d\text{hf}}$, $v^r_{q\text{hf}}$, $i^r_{d\text{hf}}$, and $i^r_{q\text{hf}}$ are the dq-axis HF voltages and currents, respectively. $R_{d\text{hf}}$, $R_{q\text{hf}}$, $L_{d\text{hf}}$, and $L_{q\text{hf}}$ are the dq-axis HF resistances and inductances, respectively.

The temperature dependencies of stator/rotor resistances R_s and remanent magnet flux B_r are [83]

$$R_{s(T_s)} = R_{s(T_0)}(1 + \alpha(T_s - T_0)), \quad (30)$$

$$B_{r(T_r)} = B_{r(T_0)}(1 + \beta(T_r - T_0)), \quad (31)$$

where T_0 is the reference temperature. T_s and T_r are the actual temperatures for stator resistance and rotor magnet. α and β are the stator copper and magnet thermal coefficients, respectively.

After measuring the stator temperature, and subtracting the stator resistive term from HF induced resistance, the PM temperature can be determined by using (30)-(31) [82]. More recently, in order to avoid the influence of magnetoresistive effect on estimation accuracy, d-axis HF inductance is used

TABLE 2. Summary of existing literature of online parameter estimation modelling techniques.

Modelling technique	Reference	Full-rank	VSI nonlinearity	Saturation effect	Estimation algorithm	Features
Fixing parameters	[97][98]	✓	✓	■	RLS	Improve performance under sensorless control.
	[108]	■	■	✓		Develop two fast and slow estimators.
	[100][101][104]	✓	■	■	EKF	Fix unestimated parameters to nominal values.
	[102]	✓	■	■		Develop reduced-order EKF.
	[103]	✓	■	■	MRAS	Utilize the similarity of chaotic system.
	[107]	✓	■	✓		Fix unestimated parameters to nominal values.
	[119]	■	■	■		Suffer from rank-deficient issue.
	[120]	✓	■	✓		Improve sensorless control at low-speed.
Invasive devices	[65]	✓	✓	■	ANN	Insert thermocouple in slots.
	[110]	✓	■	✓	-	Assemble thermal couples.
Multistep estimation	[58][59][60]	✓	■	■	-	Suffer from PM demagnetization deteriorated estimation accuracy.
Current/voltage injection	[61][62]	✓	✓	■	ANN	Analyse rank-deficient issue firstly [61].
	[63][70][73]	✓	✓	■	AIs	Estimate parameter based on global optimizations.
	[75][76]	✓	✓	✓	RLS	Consider self- and cross-saturation of inductances.
POPE	[35][66][81]	✓	✓	✓	QGA/ANN	Require stable speed and load torque if $i_d \neq 0$.
Variable speed control	[80][81]	✓	✓	✓	QGA	Specially applied to constant current control.
HF signal injection	[82][83][88]	✓	■	✓	-	Estimate PM temperature by HF rotor resistance and inductance.
	[84][85]	✓	■	✓	-	Inject two HF signals to estimate *dq*-axis inductances.
	[86][90]	✓	■	✓	-	Estimate self- and mutual HF incremental inductances.
	[89]	✓	■	✓	-	Avoid delay effect by three HF voltage injection stages.
Zero-voltage vector injection	[92]	✓	✓	■	-	Increase current ripple and high sampling rate.
Others	[78][79]	✓	■	■	-	Inject *d*-axis current and design window functions.
	[93][94]	✓	■	■	PF	Use relationship between speed-harmonic and ψ_{pm}.
	[117]	✓	✓	✓	-	Improve performance of predicted PM temperature using KF.
	[118]	✓	✓	✓	-	Require high currents sampling rate in PWM period.

"✓": considered; "■": not reported.

in [83] to estimate PM temperature, since $L_{d\text{hf}}$ is a function of d-axis magnetic saturation and temperature dependent magnet remanent flux (31). Besides, online torque estimation combined with parameter estimation is proposed in [84] based on dq-axis pulsating HF signals, which can separately estimate d-axis and q-axis inductances. In [85], HF square wave voltages in the $\alpha\beta$-axis are injected to estimate dq-axis inductances. To avoid the delay effect caused by voltage generation and digital filters, a combined rotating and pulsating HF voltage injection technique is proposed in [89] calculate dq-axis incremental inductances. Additionally, HF voltage is superimposed on the fundamental excitation in [90] to estimate self- and mutual incremental inductances, and then, together with the estimated apparent inductance, an RLS estimator is used to estimate R_s and ψ_{pm}. As above, the HF signal-based modelling techniques cannot directly estimate ψ_{pm} and is restricted to applications with a low fundamental electrical frequency.

F. OTHERS

It is worth mentioning that some papers are primarily concerned with a single parameter estimation for specific applications. Two current injection techniques, i.e. "angle" and "magnitude", are introduced to estimate R_s for thermal condition monitoring to prevent failure of the winding insulation, where a window function is developed to suppress the disturbance of the periodic current injection on the PMSM drive system [78] and [79]. By utilizing zero-voltage vector, the location of the rotor position and ψ_{pm} can be estimated from the measured current variations in the injected periods [92]. However, the additional zero-voltage vector injection will increase the current ripple. To eliminate the uncertainty of the electrical models of PMSMs and drives, [93], [94] utilize the speed harmonic to estimate ψ_{pm}. The relationship between the rotor flux linkage and the speed harmonic is built by using the machine mechanical equation. q -axis harmonic current is injected to build the full-rank reference model. However, the proposed approach requires

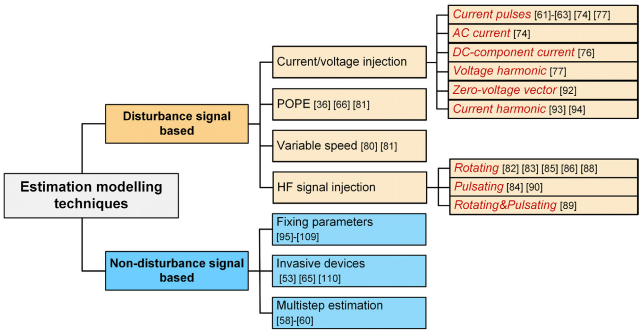

FIGURE 26. Summary of widely used estimation modelling techniques.

the accurate detection of the speed harmonic. As regard to the rotor flux linkage estimation, ψ_{pm} is estimated based on the PMSM model considering VSI nonlinearity in [117], and then the estimated rotor flux linkage can monitor the thermal condition of magnets by incorporating with KF to smooth the prediction. In [118], ψ_{pm} is estimated based on multiple sampling in each PWM period, which requires high current sampling rates.

V. SUMMARY OF LITERATURE AND EVALUATION

The different online estimation modelling techniques in the existing literature are summarised in Table 2 and presented in Fig. 26, accounting for the rank-deficient and VSI nonlinearity issues, the saturation effect, as well as the features for each method.

Table 3 summarizes the features of the main estimation modelling techniques. As aforementioned, fixing one or two parameters is the simplest method but requires the machine nominal values. Meanwhile, both temperature and saturation effects will reduce the estimation accuracy and may lead to misconvergence. Even though the actual temperatures of stator resistance and magnet can be detected via invasive thermal couples or thermal imager, direct temperature measurement is inapplicable to low-cost industrial applications due to constructional and cost issues. Multistep estimation methods are usually not dependant on nominal machine parameter values, but cannot take into account the temperature rise in PMs. The various current/voltage injection estimation methods can be used in the non-magnetic saturation conditions and are beneficial to multiple parameter estimation. Nevertheless, the periodic signal injection gives rise to the parasitic effects on the control performance, and the estimated results are sensitive to the VSI nonlinearity. In contrast, the POPE modelling method is robust against the influences of VSI and variation of parameters. However, this approach has the drawback that the position-offsets affect the rotor speed and output torque, and the rotor speed and load torque must be stable especially if $i_d \neq 0$. The parameter estimation under variable speed control is usually competitive in traction control, which can maintain constant currents and take into account the magnetic saturation. However, it is usually only applicable to the cases with constant output torque, such as traction control and wind power generation. Besides, as known from the application of HF signal to sensorless control, the injected frequency needs to be set significantly higher than the fundamental frequency.

VI. TYPICAL APPLICATIONS AND EXAMPLES

The online estimation of PMSM parameters has great significance in industrial applications. The accurate electrical and mechanical parameters can improve control performance under both sensored and sensorless control. The variations of parameters can also be used for condition monitoring and fault diagnosis.

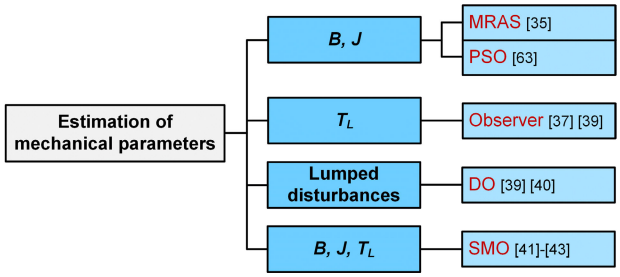

FIGURE 27. Application of online parameter estimation to determination of mechanical parameters.

A. DETERMINATION OF MECHANICAL PARAMETERS

As previously discussed, the mechanical parameters, i.e. the moment of inertia J, the friction coefficient B, and the load torque T_L, have critical effects on the dynamic performance of the speed control, and are usually dependent on the load characteristics. To date, several offline/online estimation methods have been proposed [32]–[43], which are summarised in Fig. 27.

Firstly, the no-load offline experimental estimation of mechanical parameters for induction machine is developed by utilizing the variations of impedance in [32], [33]. Sinusoidal torque input signals are developed to estimate J and B in [34], [36]. With respect to online estimation, a POPE and MRAS combined method is proposed in [35] to estimate torque constant and mechanical parameters. The mechanical parameters are estimated by two steps, i.e. estimation of B at steady state (first step) and estimation of J under sinusoidal perturbation of rotor speed (second step). The estimated results are shown in Fig. 28. The POPE has been introduced in Section IV C.

Regarding the observer-based methods, a disturbance observer (DO) for load torque estimation is designed in [38] to estimate T_L in real-time while the other mechanical uncertainties associated with the load torque are completely ignored. Considering the practical disturbances in the servo system, i.e. cogging torque, load torque, measurement errors, dead-time effect, and parameter perturbation, a DO is developed in [39] to estimate multiple disturbances. Nevertheless, since the disturbances are lumped together by utilizing DOs,

TABLE 3. Evaluation of main modelling techniques for online parameter estimation.

Modelling techniques	Advantages	Disadvantages
Fixing parameters	+ Easy implementation	– Nominal values required – Deteriorated accuracy due to parameter variation
Invasive devices	+ Capable of tracking temperature-effect of winding and PM on the parameter variation.	– Constructional drawback – Data transmission difficulty – Additional cost of devices
Multistep estimation	+ Easy implementation + Do not require nominal values	– Temperature effect of PM is not considered – Sensitive to VSI nonlinearity
Current/voltage injection	+ Do not require nominal values + Capable of acquiring multiple parameters	– Magnetic saturation effect is usually ignored – Sensitive to VSI nonlinearity – Increased computational burden – Parasitic effect on control performance
POPE	+ Independent of magnetic saturation + Independent of VSI nonlinearity	– Only rotor flux linkage can be estimated – Rotor speed and load torque must be stable if $i_d \neq 0$
Variable speed control	+ Capable of considering magnetic saturation effect	– Only applicable under constant current control
HF signal injection	+ Capable of tracking PM ageing effect + Good performance at low speed	– Increased harmonics and losses – Not applicable at high fundamental frequency

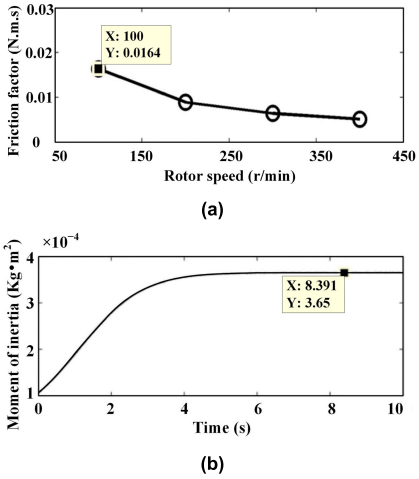

FIGURE 28. MRAS estimated mechanical parameters [35]. (a) Friction factor B. (b) Moment of rotor inertia (nominal value: 3.52×10^{-4}kg· m^2).

it is difficult to identify the individual parameter uncertainty. Additionally, to mitigate the phase lag and the amplitude attenuation caused by a low-pass filter (LPF), the authors in [40] develop an extended SMO-based method to estimate B, J and T_L without incurring phase lag. A second-order terminal sliding-mode observer (SMO) is proposed to estimate mechanical parameters, such as B, J and T_L, and achieves fast convergence in finite time [41]. In [42], a SMO based observer and two-moment of inertia estimation methods are developed to estimate B, J and T_L, where the estimation error of load torque due to mismatches of the mechanical parameters are considered. To identify the load torque under variable-speed or variable-load servo drive system, an improved adaptive SMO is proposed in [43]. The descriptions of DO and SMO can be found in Appendix G.

B. IMPROVEMENT OF CONTROL PERFORMANCE

As is well known, the machine parameters are strongly affected by operating and environmental conditions [76], and consequently, the inaccurate estimation of machine parameters will deteriorate the control performance. Fig. 29 presents the applications of online parameter estimation to the control performance improvement.

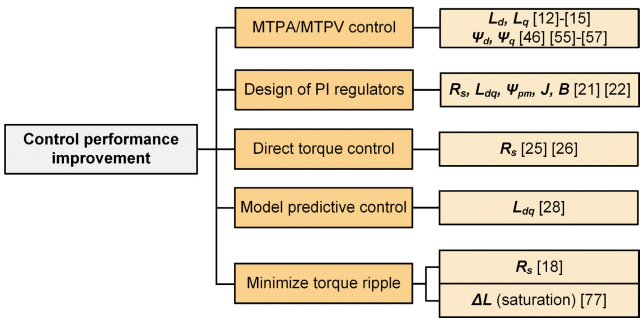

FIGURE 29. Application of online parameter estimation to control performance improvement.

Regarding the most popular FOC, the PI regulators in the current and speed control loops need accurate machine parameters. L_d, L_q, R_s are essential for the design of PI constants of current loop regulator; while ψ_{pm} and mechanical parameters, such as B and J, are essential for the design of the PI constants for the speed loop regulator. Moreover, it has

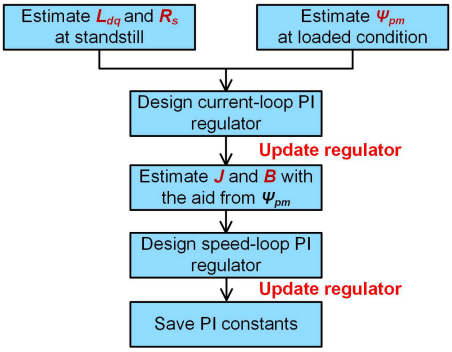

FIGURE 30. Flowchart of design speed- and current-loop PI regulators [21].

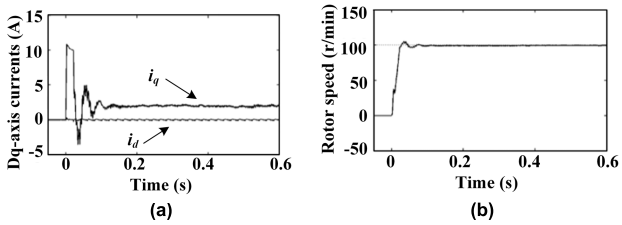

FIGURE 31. Responses of PI regulators from step change of rotor speed [21].

been reported in [21], [22] that with the aid of multiple parameter estimation, the optimized PI regulators can be easily determined. The flowchart of PI controller design is presented in Fig. 30. The experimental performance of the step response of rotor speed from 0 r/min to 100 r/min is shown in Fig. 31. It is evident that the designed PI regulator can achieve small overshoot and fast response of q-axis current.

DTC has many advantages such as lower machine parameter dependence, simpler implementation and faster dynamic torque response [23], [24]. However, accurate knowledge of the stator resistance is required to estimate the stator flux vector and electromagnetic torque [25], [26]. If R_s is under-estimated in the DTC system, the drive system will tend to be unstable due to additional energy flowing into the machine. Consequently, the accumulated energy will reduce the system's stability.

Additionally, model predictive control (MPC) is another high-performance control method after FOC and DTC, and has unique advantages, e.g. fast response, flexible and no static error and overshoot. However, MPC is sensitive to parameters [27]–[31]. In [28], instead of using a conventional offline look-up table, the RLS estimator is used to online estimate the incremental stator inductances by considering the magnetic saturation effects under FCS-MPC system. Moreover, observer-based MPC methods for induction machines are proposed in [29]–[31], which shows good robustness against load disturbance and parameter uncertainties.

Besides, to minimize the torque ripple for PMSM drive systems caused by asymmetric phase resistances, flux and current harmonics, etc., the RLS, the adaptive observer-based, the ANN estimators [18], and the harmonic injection-based method [77], are developed to identify stator resistance, load torque, inductances, and optimal current, respectively.

C. SENSORLESS CONTROL

Sensorless PMSM drives have been receiving increased interest for use in industrial applications since they do not need position sensors, and thus, reduce the cost and size of the drive system while increasing the overall system reliability [58], [120]. Generally, the sensorless control can be classified into two basic categories: the PMSM model-based and the rotor-saliency-based techniques.

To estimate the rotor position information, the PMSM model-based sensorless control method does not rely on the additional signal injection and usually utilizes the back-EMF vector [55], [74], [95], [98], [107], [121], or the rotor flux vector [58], [101], [122]–[124]. However, the model-based method is sensitive to the variation of electrical parameters and degraded at both standstill and low speed. To date, numerous papers have been published to deal with the online estimation of uncertain parameters under sensorless control schemes, as shown in Fig. 32 and described as follows.

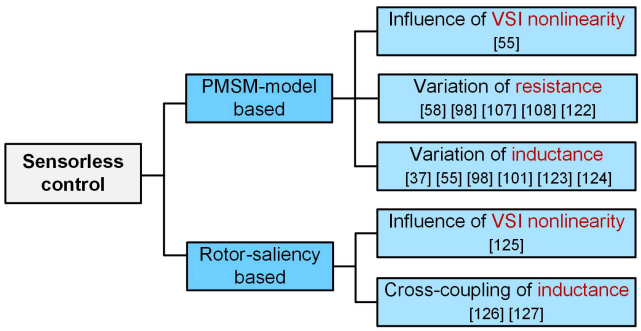

FIGURE 32. Application of online parameter estimation to sensorless control.

Firstly, [55] investigates the influence of the voltage compensation and the parameter variation on the performance of the back-EMF based sensorless control, where the nonlinearity of VSI and the variation of L_q are identified based on the RLS estimator. Besides, the stator resistance is the most sensitive parameter at the low-speed range, and the inaccurate value will result in large position error and instability risks. Hence, the MRAS [58], [107], RLS estimators [98], [108], and the reduced-order observer [122], are used to adapt stator resistance under sensorless control. Meanwhile, the variation of dq-axis inductances caused by magnetic saturation is the other issue for sensorless control and regardless of the rotor speed [98]. The decrease of stator inductances due to magnetic saturation will give rise to a lagged estimation error of the rotor position. The inaccurate current distribution in the dq-axis coordinates will further deteriorate the estimation accuracy. The online inductance estimation methods including RLS [55], [98], [108], the EKF [101] and the observers [37], [123] and [124].

The rotor-saliency-based or magnetic saturation induced saliency-based method usually requires the injection of HF signal into the phase windings and then measuring and controlling the resultant HF current, which is often used for starting and low-speed operation. However, it has been reported in [125], [126] that the VSI nonlinearity and the cross-coupling magnetic saturation could cause an estimation error of the rotor position. In [127], an improved signal-injection-method is proposed by compensating for the cross-coupling magnetic saturation effect from the pre-FEA calculated or pre-measured incremental mutual inductances. Fig. 33 compares the position estimation errors between the conventional and improved methods.

D. THERMAL CONDITION MONITORING

The online thermal condition monitoring of PMSMs is essential to the safe operation, the machine life-time and the improved control performance, particularly for the most vulnerable components of PM and the stator winding [6]. More specifically, the winding insulation will be damaged when the winding temperature exceeds the allowed temperature. Meanwhile, when the PM temperature exceeds its Curie temperature, it will cause irreversible partial demagnetization [129]–[132].

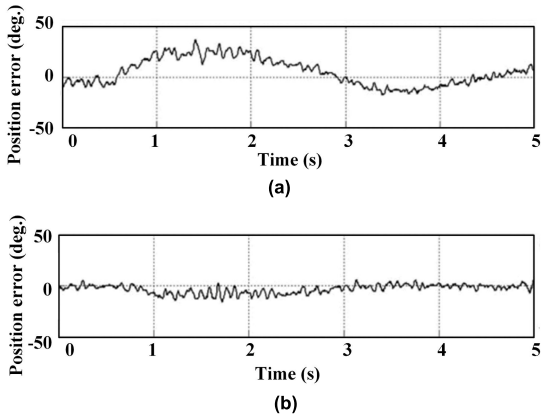

FIGURE 33. Measured rotor position errors [127]. (a) Conventional method. (b) Improved method considering magnetic saturation.

The direct measurement of PM temperature under load condition is still challenging since it is usually not practical for thermal sensors to have a direct contact on the rotating rotor PMs. To date, several methods and devices have been developed to directly measure the PM temperature, i.e. infrared thermal imager and thermometer (limited to the PM visibility), standard thermal sensors combined with wireless data transmission devices [87], [88], [131], and [132]. Nevertheless, these approaches are not feasible in the industrial applications due to additional costs, constructional drawbacks and risks of sensor failures [7].

Against the above background, the temperature dependencies of the stator resistance and the rotor flux linkage are used for the thermal indicators to monitor thermal conditions indirectly and expressed as

$$R_{s,s} = R_{s,0}\left[1 + \alpha(T_s - T_0)\right], \tag{32}$$

where $R_{s,s}$ and $R_{s,0}$ are the stator resistances at the actual temperature T_s and the reference temperature T_0. α is the temperature coefficient of copper.

$$\psi_{pm,s} = \psi_{pm,0}\left[1 + \beta(T_{pm} - T_0)\right], \tag{33}$$

where $\psi_{pm,s}$ and $\psi_{pm,0}$ are the rotor flux linkages at the actual temperature T_{pm} and the reference temperature T_0. β is the temperature coefficient of remanent flux density.

TABLE 4. Temperature characteristics of typical PM materials [7], [128].

Property	Ferrite	NdFeB	SmCo	AlNiCo
BH_{max} [kJ/m^3]	10~42	200~400	150~230	35~60
T_{max} [°C]	300	150~230	250	450
α_{B_r} [%/°C]	-0.2	-0.15~-0.1	-0.06~-0.02	-0.03
α_{H_C} [%/°C]	0.2~0.5	-0.6~-0.4	-0.4~-0.2	0.2
ρ [Ω·cm]×10^{-6}	10^4	110-170	50-90	50-80

Table 4 shows the physical properties of some typical PM materials, where BH_{max} and T_{max} are the maximum energy product and the maximum operating temperature; α_{B_r} and α_{H_C} are the temperature coefficients of remanent flux density and the coercive field strength, respectively; ρ is the electrical resistivity. The negative α_{H_C} means that the materials are more vulnerable to irreversible magnet demagnetization.

In order to amplify the resistive voltage drop and increase the resolution of the estimated stator resistance, two current injection methods are proposed in [78], [79]. Meanwhile, the other online parameter estimation techniques, e.g. AIs [62], [76]–[81], HF signal injection based methods [82], [83] and [88], as well as EKF [102], [133], are able to track thermal states of the stator winding and the rotor magnet by utilizing the temperature correlations (32)-(33). For instance, the estimated values of R_s and ψ_{pm} based on ANN algorithm [62] at the initial thermal state and after heating are presented in Fig. 34. As can be seen, after heating of 20 minutes, the estimated stator resistance increases from 0.388 Ω to 0.473 Ω, while the rotor flux linkage decreases from 78.8 mWb to 73 mWb.

E. FAULT DIAGNOSIS

The online parameter estimation techniques are widely used in detecting fault-related signals and do not rely on additional measurement devices [1]–[3]. The most prevalent faults of PMSMs can be categorized as follows, while the corresponding applications of online parameter estimation are shown in Fig. 35.

1) Electrical faults including short/open circuit faults.
2) PM demagnetization faults.
3) Mechanical faults including bearing faults and static/dynamic eccentricity faults.

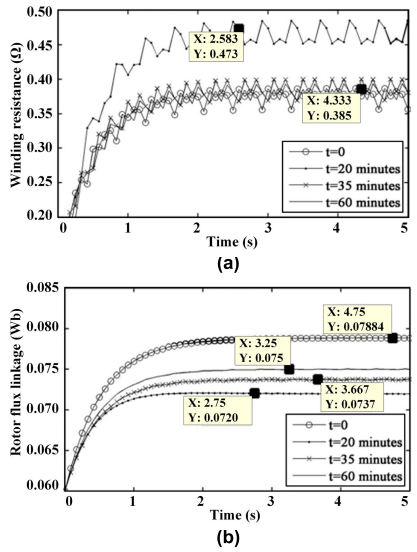

FIGURE 34. Stator resistance and rotor flux linkage at initial thermal states and after heating [62]. (a) Estimated stator resistance. (b) Estimated rotor flux linkage.

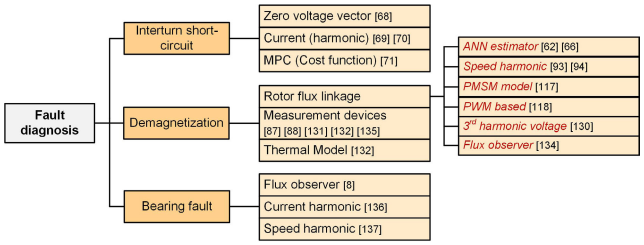

FIGURE 35. Application of online parameter estimation to fault diagnosis.

Firstly, the interturn short-circuit (ITSC) fault is most common among all electrical faults and is usually caused by mechanical stress, moisture, and partial discharge [67]–[71]. As this fault occurs, a high circulating current is generated in the shorted circuit, which may propagate and further lead to phase-to-phase, phase-to-ground, and demagnetization faults. A comprehensive short-circuit current analysis under different fault scenarios can be found in [67] based on the FEA model, where the fault resistance in the short-circuit path is considered. In [68], a zero-sequence voltage vector-based method is proposed to address the ITSC in low-speed PMSMs. Reference [69] proposes an online ITSC detecting method by utilizing the second-order harmonics in the q-axis current in comparison to the non-fault condition. Reference [70] proposes a stator fault detection method by utilizing the stator current difference between the measured and observer estimated stator currents, where the disturbances caused by parameter uncertainties, asymmetric stator and measurement noises are decoupled to avoid false alarms. For model-predictive controlled PMSM, an ITSC fault diagnosis method is proposed in [71] based on the cost function and wavelet transform, where discrete wavelet transfer (DWT) is used to extract the characteristic fault features.

Secondly, as mentioned above, PM demagnetization will deteriorate characteristics of the PM and result in the decrease of output torque. The PM demagnetization is usually caused by physical damage, high-temperature stress, inverse magnetic field and ageing. Since the rotor flux linkage is proportional to the strength, the online parameter estimation of the rotor flux linkage is widely used to detect demagnetization faults and to evaluate the degree of demagnetization accounting for the variations of L_d, L_q and R_s [93], [94], and [118]. In addition, a measurement method for detecting rotor eccentricity and local demagnetization for PMSM is proposed with the aim of the analog Hall-effect field sensors [135].

Regarding bearing faults, they might manifest themselves as rotor asymmetry faults [2], [3]. Otherwise, the ball bearing related defects can be categorized as an outer bearing race defect, an inner bearing race defect, a ball defect, or a train defect. The vibration monitoring of mechanical characteristic frequencies related to the bearings is widely used to detect faulty operation. However, vibration measurement suffers from additional cost and is not always feasible in industrial applications. Hence, the stator current and speed harmonic are used as fault signals to diagnose bearing faults. For instance, to overcome the difficulty of extracting the weak characteristic fault current signals, a full-order flux linkage observer and improved analysis method of flux linkage peak energy spectrum are proposed in [8], which can diagnose different types of bearing faults for traction motor accurately (e.g. outer/inner ring, rolling element, etc.), and it is of practical significance in the engineering field. Moreover, an online current signal based ANN is proposed in [136] to diagnose the bearing faults for induction machines, while a Luenberger speed observer is employed in [137] to perform speed harmonic detection for bearing fault diagnosis in an induction machine.

VII. OUTLOOK OF FUTURE RESEARCH TRENDS

According to the above overview, the techniques of online parameter estimation have great research potential. The future research trends could be initiated from the following aspects:

1) As introduced before, the estimation of stator inductances and rotor flux linkage considering the magnetic saturation effect is still mainly based on the extensive offline machine identification. Thus, online determination of the magnetic saturation level is worth further investigating.
2) Novel estimation modelling techniques could be further investigated to improve the robustness against the influence of VSI nonlinearity and measurement errors.
3) Application of online parameter estimation to the state-of-the-art control strategies to achieve better control performance and higher efficiency, e.g. finite-control-set MPC and DTC, etc.
4) Application of different estimation modelling techniques for special machines is one of the valuable research tendencies, e.g. dual three-phase machines,

open-winding machines, synchronous reluctance machines, variable flux memory machine, etc.

5) Application of online parameter estimation to sensorless PMSM drives.

VIII. CONCLUSION

The state-of-the-art techniques of online parameter estimation of PMSMs have been systemically overviewed in this paper together with extensive examples. Firstly, the critical rank deficient and ill- issues were emphasized and analysed. Secondly, the widely used modelling techniques for PMSM parameter estimation, i.e. multistep estimation, current/voltage injection, POPE, estimation under variable speed control, as well as the HF signal injection, were highlighted, in terms of with/without considering saturation and temperature effects. Some typical industrial applications were described, again, with examples, including determination of mechanical parameters, performance improvement under sensored and sensorless control, thermal condition monitoring, as well as fault diagnosis. Finally, some future research trends were predicted. The online parameter estimation techniques overviewed are also applicable to induction machines and synchronous reluctance machines.

APPENDICES

The most common modern estimation algorithms are described in Appendices A-G and evaluated in Appendix H.

A. RLS ALGORITHM

Due to its easy implementation and good convergence properties, the RLS estimator is widely used in the online parameter estimation [75], [76]. RLS is a numerical algorithm to recursively estimate the parameters by minimizing the weighted least square cost functions relating to the observed and computed signals [138].

Firstly, it is assumed that the model is expressed as

$$y = \Phi x, \tag{A.1}$$

where y and x are the output and input matrices. Φ is the unknown parameters vector of the model.

By minimizing the least square of the predicted errors ε_i, the objective function is defined as

$$\varepsilon_k = \left(y_k - \hat{\Phi}^T x_k\right)^2, \tag{A.2}$$

where $\hat{\Phi}$ is the unknown parameter vector.

The updating algorithm is calculated as

$$\hat{\Phi}_k = \hat{\Phi}_{k-1} + K_k\left(y_k - x_k^T\hat{\Phi}_{k-1}\right), \tag{A.3}$$

$$K_k = P_{k-1}x_k(\lambda I + x_k^T P_{k-1}x_k)^{-1}, \tag{A.4}$$

$$P_k = \frac{P_{k-1}}{\lambda}(I - K_k x_k^T), \tag{A.5}$$

where K_k is the gain matrix. λ is the weighting coefficient. P_k is the covariance matrix. The subscripts $k/k-1$ denote sampling index. Since the RLS estimator uses the fixed gain, the accuracy of the estimation is not guaranteed without the parameter variation.

B. EKF ALGORITHM

The estimation process of the Kalman/extended Kalman filter (KF/EKF) is similar to the RLS. The RLS updates the estimation of a static parameter, while KF is able to update and estimate an evolving state. Its main feature is the recursive processing of the noise measurement risk [139], [140]. Since the conventional KF cannot directly estimate the states for non-linear systems, it extends to EKF by utilizing the first order Taylor series for linearization. The EKF based estimator is shown in Fig. 36.

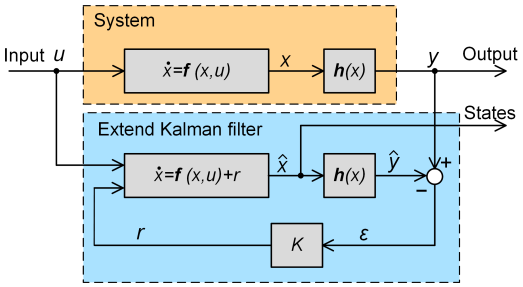

FIGURE 36. Schematic parameter estimation based on EKF.

The nonlinear state equations are written as

$$x_{k+1} = \boldsymbol{f}(x_k, u_k) + w_k, \tag{A.6}$$

$$y_k = \boldsymbol{h}(x_k) + v_k, \tag{A.7}$$

where $\boldsymbol{f}$ is the function of a nonlinear system. u is the control vector. w and v are the zero-mean white Gaussian system and measurement noises with covariances Q and R, respectively. $w(t)$ takes into account the system disturbances and model inaccuracies while $v(t)$ considers measurement errors.

Generally, EKF based estimation has two steps: the prediction step and the update step.

1) Prediction step

$$\begin{cases} \hat{x}_{k+1|k} = f\left(\hat{x}_{k|k}, u_k\right), \\ P_{k+1|k} = A_k P_{k|k} A_k^T + Q. \end{cases} \tag{A.8}$$

1) Update step

$$\begin{cases} K_{k+1} = P_{k+1|k}H_k^T\left[H_k P_{k+1|k} H_k^T + R\right]^{-1}, \\ \hat{x}_{k+1|k+1} = \hat{x}_{k+1|k} + K_{k+1}(y_{k+1} - \boldsymbol{h}(\hat{x}_{k+1|k})) \\ P_{k+1|k+1} = (I - K_{k+1}H_k)\,P_{k+1|k}, \end{cases} \tag{A.9}$$

$$A_k = \left.\frac{\partial \boldsymbol{f}(x,u)}{\partial x}\right|_{x=\hat{x}_k},$$

$$H_k = \left.\frac{\partial \boldsymbol{h}(x)}{\partial x}\right|_{x=\hat{x}_k}, \tag{A.10}$$

where A_k and H_k are the Jacobian matrices of the partial derivatives of $\boldsymbol{f}$ and $\boldsymbol{h}$ with respect to x and need to be updated in every sampling period. However, the EKF may fail to converge on the appropriate state values if the system model is

inaccurate. The computational burden increases significantly as the order of system increases due to inverse matrix calculation. It processes input data with noise repeatedly which may also lead to a high computational burden [45].

C. MRAS AND AO ALGORITHMS

Firstly, adaptive MRAS is widely used in the sensorless control and online parameter estimation due to its guaranteed convergence and simple form with less computation burden [105]. The structure of the MRAS is shown in Fig. 37.

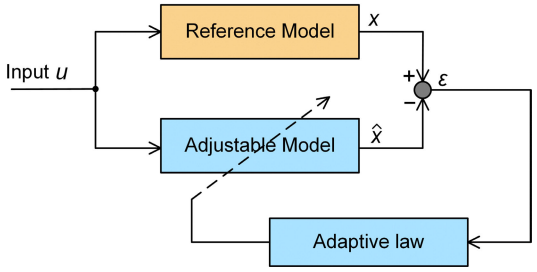

FIGURE 37. Structure of model reference adaptive algorithm.

The MRAS estimator includes the reference model, the independent adjustable model and the adaptive law, in which the estimation error ε between the reference model x and the adjustable model $\hat{x}$ is calculated, and then fedback to the proper adaptive law to adjust the values of the estimated parameters.

Similar to the MRAS algorithm, the principle of AO is to build an adjustable model with parameters to be estimated and a reference model (practical machine). By utilizing the appropriate adaptive law, the output difference between two models, e.g. values of current/flux, are adjusted adaptively until convergence.

The adaptive laws include the MIT rule, the Popov stability criterion and the Lyapunov stability theorem. The MIT rule is the simplest one but suffers from instability risks. In [119], a MIT rule-based MRAS is proposed to estimate multi-parameters, such as iron loss and stator resistances, stator inductances, back EMF, as well as the viscous and inertia constant. However, the MIT rule-based MRAS system lacks stability design and is not feasible for practical applications. Thus, the latter two adaptive laws are widely used. On the one hand, by using the Popov stability criterion, the system can be transferred into a nonlinear time variable feedback system. On the other hand, the Lyapunov stability theorem based MRAS estimator relies on the individual Lyapunov function, which requires an experienced designer. In comparison, the Popov based MRAS estimator exhibits better performance in practice due to its easy design process.

D. PSO ALGORITHM

The PSO algorithm is a nature inspired algorithm and was first proposed by Kennedy and Eberhart in 1995 [142]. The structure of the PSO based parameter estimation approach can be illustrated in Fig. 38.

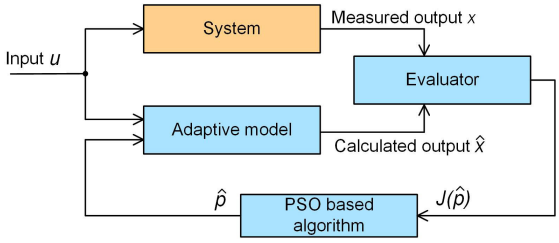

FIGURE 38. Structure of PSO algorithm based parameter estimation.

The PSO algorithms, e.g. improved PSO, self-learning PSO (SLPSO), etc., have been widely used in the multi-dimensional optimization and parameter estimation due to its fast convergence. The standard PSO is taken as an example and its updating rule is described as

$$v_{i+1} = wv_i + c_1 r_1 \left(x_p - x_i\right) + c_2 r_2 \left(x_g - x_i\right), \quad \text{(A.11)}$$

$$x_{i+1} = x_i + v_i, \quad \text{(A.12)}$$

where w is the inertia weight. c_1, c_2 are the cognitive and social acceleration constants, respectively. x_p, x_g are the particle best and overall best locations, respectively. x_i is the ith particle location. v_i represents the particle velocity. r_1 and r_2 are the random numbers between 0 and 1. The general steps of PSO for the parameter estimation are written as follows.

Algorithm 1 PSO Algorithm for Parameter Estimation

Step 1: Initialization
Initialize parameters, optimization settings (number of particle, maximum iterative number, terminal conditions).

Step 2: Data loading
Load measured data for parameter estimation.

Step 3: Update speed and position
Update particle's velocity in (A.11).
Update particle's position in (A.12).

Step 4: Update best personal and global best positions
If $Fit(x_i) < Fit(x_p)$, then update $x_p \leftarrow x_i$
If $Fit(x_p) < Fit(x_g)$, then update $x_g \leftarrow x_p$

Step 5: Evaluation
Evaluate the fitness of the global best position and the iterative number, if not satisfy the terminal condition, return to step 3, else go to step 6.

Step 6: Output estimated parameters

E. ANN

In comparison to the aforementioned estimators, i.e. EKF and MRAS, the Adaline NN (ANN) algorithm requires less computation time and convergence is achieved more quickly.

The mathematical model of the ANN is expressed as

$$O\left(W_i, X_i\right) = \sum_{i=0}^{n} W_i X_i, \quad \text{(A.13)}$$

where W_i is the net weight and X_i is the input signal.

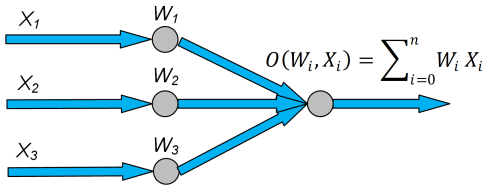

FIGURE 39. Structure of an adaline NN.

The structure of the ANN is shown in Fig. 39. The activation function $O(W_i, X_i)$ of the network output node is a linear function. The objective function is defined as minimizing the sum of squared errors, and thus, the updated W_i in each sampling period is presented as

$$W_{i,k+1} = W_{i,k} + 2\eta X_i(\hat{O}_k - O_k), \tag{A.14}$$

where η is the convergence factor adjusting the convergence speed. $\hat{O}_k$ is the predicted output. k and $k+1$ are the sampling indexes. The convergence factor η is limited to a proper range of values.

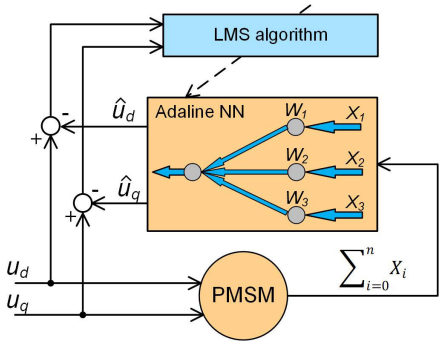

FIGURE 40. Complete adaline NN based parameter estimation for PMSM.

Fig. 40 shows the complete ANN based estimation system for PMSM. The least mean square (LMS) algorithm is used to minimize the predicted and measured errors. The detailed introduction of ANN can be found in [143].

F. GA

The process of parameter estimation by GAs is similar to the PSO based estimator (see Fig. 38) and usually consists of three steps [144]–[145].

1) **Initialization.** During the initialization of EA, a group of solutions for cost functions will be generated randomly, which is designated as the gene pool of a population. These solutions are generated in the form of gene encoding.
2) **Iterative evolution.** All solutions will be processed by various evolutionary operators, by which the optimal or suboptimal solutions will be randomly worked out.
3) **Termination.** The evolution will be terminated if the global optimal is obtained or the algorithm has reached the maximum generation of evolution.

Therefore, GA is one of the most popular EAs and widely employed in real industrial applications. Quantum GA (QGA) is an improvement of GA and has superior performance in the preservation of good solutions and quantum binary encoding [144]. The procedures of the conventional QGA are introduced as follows:

Algorithm 2 QGA for Parameter Estimation

Step 1: Initialization
Initialize parameters, optimization settings (initial population, maximum generation number, etc.)

Step 2: Selection operator
A subpopulation is randomly selected to breed a new generation in each successive generation.

Step 3: Crossover operator
Gene information will be interchanged by probability, and no new gene bit generates in this operator.

Step 4: Mutation operator
New gene bits will be generated by mutation probability.

Step 5: Quantum rotation gate operator
This operator makes the genes converge to the fitter states.

Step 6: Termination
Judge whether the termination condition is satisfied go to Step 7, or else return to Step 2.

Step 7: Output estimated parameters

G. DO AND SMO

DOs are widely used to estimate the disturbances of a PMSM drive system, i.e. unmodeled dynamics, parametric uncertainties, and external disturbances [146]. The schematic diagram of a DO based control system is shown in Fig. 41.

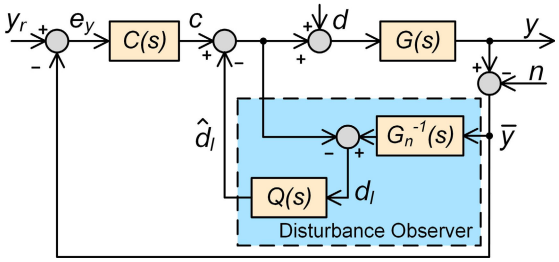

FIGURE 41. Schematic diagram of DO based control system [146].

$G(s)$ and $G_n(s)$ represent the real physical plant and the nominal model used for the controller design. $Q(s)$ is a stable filter. u is the control input. c is the feedback controller output. y_r is the reference signal. y and $\bar{y}$ are the system and measured outputs, respectively. n is the measurement noise. d, d_l, and $\hat{d}_l$ are the external, actual lumped, and estimated disturbances, respectively. The nominal plant $G_n(s)$ is preserved in the absence of the disturbance and uncertainty, and therefore, the control system can be regarded as a classical feedback loop with the controller $C(s)$. However, the inner loop will be activated in the presence of uncertainty to suppress the influence of uncertainty.

SMO is an observer with inputs as discontinuous functions of the error between the estimated and measured outputs, and has its unique advantages, i.e. high robustness to the disturbances and the system parameter variations [147], [148]. The essence of the SMO is a HF switching feedback control, which is composed of two parts, i.e. sliding surface and control law. The system states can be switched by utilizing signum function, sigmoid function, power function, etc.

H. EVALUATION OF ESTIMATION ALGORITHMS

As a summary, the characteristics of presented algorithms are evaluated in Table 5.

TABLE 5. Major pros and cons of parameter estimation algorithms.

Methods	Pros	Cons
RLS	Easy implementation	Sensitive to noise
EKF	Robust to noise	Complicated computation
MRAS	Simple structure	Complicated design
AO	Good applicability	Complicated design
DO	Robust control	All disturbances lumped
SMO	Robust to noise	Chattering problem
ANN	Easy implementation	Persistent excitation
SPO	Multiparameter estimation	High computational burden
EA	Multiparameter estimation	High computational burden

REFERENCES

[1] Z. Q. Zhu and D. Howe, "Electrical machines and drives for electric, hybrid, and fuel cell vehicles," *Proc. IEEE*, vol. 95, no. 4, pp. 746–765, Apr. 2007.
[2] Z. Gao, C. Cecati, and S. X. Ding, "A survey of fault diagnosis and fault-tolerant techniques—Part I: Fault diagnosis with model-based and signal-based approaches," *IEEE Trans. Ind. Electron.*, vol. 62, no. 6, pp. 3757–3767, Jun. 2015.
[3] Z. Gao, C. Cecati, and S. Ding, "A survey of fault diagnosis and fault-tolerant techniques—Part II: Fault diagnosis with knowledge-based and hybrid/active approaches," *IEEE Trans. Ind. Electron.*, vol. 62, no. 6, pp. 3757–3767, Jun. 2015.
[4] X. Liu, H. Chen, J. Zhao, and A. Belahcen, "Research on the performances and parameters of interior PMSM used for electric vehicles," *IEEE Trans. Ind. Electron.*, vol. 63, no. 6, pp. 3533–3545, Jun. 2016.
[5] M. Tursini, F. Parasiliti, and D. Zhang, "Real-time gain tuning of PI controllers for high-performance PMSM drives," *IEEE Trans. Ind. Appl.*, vol. 38, no. 4, pp. 1018–1026, Jul./Aug. 2002.
[6] A. Boglietti, A. Cavagnino, D. Staton, M. Shanel, M. Mueller, and C. Mejuto, "Evolution and modern approaches for thermal analysis of electrical machines," *IEEE Trans. Ind. Electron.*, vol. 56, no. 3, pp. 871–882, Mar. 2009.
[7] O. Wallscheid, T. Huber, W. Peters, and J. Böcker, "A critical review of techniques to determine the magnet temperature of permanent magnet synchronous motors under real-time conditions," *EPE J.*, vol. 26, no. 1, pp. 11–20, Aug. 2016.
[8] J. H. Feng, "Fault diagnosis method of traction motor bearing based on improved flux peak energy spectrum," *J. Central South Univ.*, early access, pp. 1–9, Jul. 2020. [Online]. Available: http://kns.cnki.net/kcms/detail/43.1426.N.20200727.1016.002.html
[9] M. Khayamy and H. Chaoui, "Current sensorless MTPA operation of interior PMSM drives for vehicular applications," *IEEE Trans. Veh. Technol.*, vol. 67, no. 8, pp. 6872–6881, Aug. 2018.
[10] L.-J. Cheng and M.-C. Tsai, "Robust scalar control of synchronous reluctance motor with optimal efficiency by MTPA control," *IEEE Access*, vol. 9, pp. 32599–32612, 2021.
[11] K. D. Hoang, P. Lazari, K. Atallah, J. G. Birchall, and S. D. Calverley, "Evaluation of simplified model for rapid identification and control development of IPM traction machines," *IEEE Trans. Transport. Electrific.*, early access, Sep. 14, 2020, doi: 10.1109/TTE.2020.3023888.
[12] Y. A.-R.-I. Mohamed and T. K. Lee, "Adaptive self-tuning MTPA vector controller for IPMSM drive system," *IEEE Trans. Energy Convers.*, vol. 21, no. 3, pp. 636–644, Sep. 2006.
[13] M. A. Rahman, D. M. Vilathgamuwa, M. N. Uddin, and K.-J. Tseng, "Nonlinear control of interior permanent-magnet synchronous motor," *IEEE Trans. Ind. Appl.*, vol. 39, no. 2, pp. 408–416, Apr. 2003.
[14] T. Senjyu, Y. Noguchi, N. Urasaki, A. Yona, and H. Sekine, "Parameter identification for interior permanent-magnet synchronous motor," in *Proc. Int. Conf. Elect. Mach. Syst. (ICEMS)*, Seoul, South Korea, 2007, pp. 566–571.
[15] M. N. Uddin and M. M. I. Chy, "Online parameter-estimation-based speed control of PM AC motor drive in flux-weakening region," *IEEE Trans. Ind. Appl.*, vol. 44, no. 5, pp. 1486–1494, Sep./Oct. 2008.
[16] Z. Li and H. Li, "MTPA control of PMSM system considering saturation and cross-coupling," in *Proc. 15th Int. Conf. Elect. Mach. Syst. (ICEMS)*, Sapporo, Japan, 2012, pp. 1–5.
[17] P. Niazi, H. A. Toliyat, and A. Goodarzi, "Robust maximum torque per ampere (MTPA) control of PM-assisted SynRM for traction applications," *IEEE Trans. Veh. Technol.*, vol. 56, no. 4, pp. 1538–1545, Jul. 2007.
[18] Y. Xu, N. Parspour, and U. Vollmer, "Torque ripple minimization using online estimation of the stator resistances with consideration of magnetic saturation," *IEEE Trans. Ind. Electron.*, vol. 61, no. 9, pp. 5105–5114, Sep. 2014.
[19] H. Kim, J. Hartwig, and R. D. Lorenz, "Using on-line parameter estimation to improve efficiency of IPM machine drives," in *Proc. IEEE 33rd Annu. IEEE Power Electron. Spec. Conf.*, Jun. 2002, pp. 815–820.
[20] T. M. Jahns and W. L. Soong, "Pulsating torque minimization techniques for permanent magnet AC motor drives—A review," *IEEE Trans. Ind. Electron.*, vol. 43, no. 2, pp. 321–330, Apr. 1996.
[21] K. Liu and Z. Q. Zhu, "Parameter estimation of PMSM for aiding PI regulator design of field oriented control," in *Proc. 17th Int. Conf. Electr. Mach. Syst. (ICEMS)*, Hangzhou, China, Oct. 2014, pp. 2705–2711.
[22] K. Liu and Z. Zhu, "Fast determination of moment of inertia of permanent magnet synchronous machine drives for design of speed loop regulator," *IEEE Trans. Control Syst. Technol.*, vol. 25, no. 5, pp. 1816–1824, Sep. 2017.
[23] L. Zhong, M. F. Rahman, W. Y. Hu, and K. W. Lim, "Analysis of direct torque control in permanent magnet synchronous motor drives," *IEEE Trans. Power Electron.*, vol. 12, no. 3, pp. 528–536, May 1997.
[24] L. Zhong, M. F. Rahman, W. Y. Hu, K. W. Lim, and M. A. Rahman, "A direct torque controller for permanent magnet synchronous motor drives," *IEEE Trans. Energy Convers.*, vol. 14, no. 3, pp. 637–642, Sep. 1999.
[25] Y. Sangsefidi, S. Ziaeinejad, A. Mehrizi-Sani, H. Pairodin-Nabi, and A. Shoulaie, "Estimation of stator resistance in direct torque control synchronous motor drives," *IEEE Trans. Energy Convers.*, vol. 30, no. 2, pp. 626–634, Jun. 2015.
[26] Y. Inoue, S. Morimoto, and M. Sanada, "Comparative study of PMSM drive systems based on current control and direct torque control in flux-weakening control region," *IEEE Trans. Ind. Appl.*, vol. 48, no. 6, pp. 2382–2389, Nov. 2012.
[27] M. Siami, D. A. Khaburi, and J. Rodriguez, "Simplified finite control set-model predictive control for matrix converter-fed PMSM drives," *IEEE Trans. Power Electron.*, vol. 33, no. 3, pp. 2438–2446, Mar. 2018.
[28] A. Brosch, S. Hanke, O. Wallscheid, and J. Böcker, "Data-driven recursive least squares estimation for model predictive current control of permanent magnet synchronous motors," *IEEE Trans. Power Electron.*, vol. 36, no. 2, pp. 2179–2190, Feb. 2021.
[29] J. Wang, F. Wang, Z. Zhang, S. Li, and J. Rodriguez, "Design and implementation of disturbance compensation-based enhanced robust finite control set predictive torque control for induction motor systems," *IEEE Trans. Ind. Informat.*, vol. 13, no. 5, pp. 2645–2656, Oct. 2017.
[30] F. Wang, J. Wang, R. M. Kennel, and J. Rodríguez, "Fast speed control of AC machines without the proportional-integral controller: Using an extended high-gain state observer," *IEEE Trans. Power Electron.*, vol. 34, no. 9, pp. 9006–9015, Sep. 2019.
[31] J. Wang, F. Wang, G. Wang, S. Li, and L. Yu, "Generalized proportional integral observer based robust finite control set predictive current control for induction motor systems with time-varying disturbances," *IEEE Trans. Ind. Informat.*, vol. 14, no. 9, pp. 4159–4168, Sep. 2018.

[32] W.-M. Lin, T.-J. Su, and R.-C. Wu, "Parameter identification of induction machine with a starting no-load low-voltage test," *IEEE Trans. Ind. Electron.*, vol. 59, no. 1, pp. 352–360, Jan. 2012.

[33] R. Babau, I. Boldea, T. J. E. Miller, and N. Muntean, "Complete parameter identification of large induction machines from no-load acceleration–deceleration tests," *IEEE Trans. Ind. Electron.*, vol. 54, no. 4, pp. 1962–1972, Aug. 2007.

[34] F. Andoh, "Moment of inertia identification using the time average of the product of torque reference input and motor position," *IEEE Trans. Power Electron.*, vol. 22, no. 6, pp. 2534–2542, Nov. 2007.

[35] K. Liu and Z. Q. Zhu, "Mechanical parameter estimation of permanent-magnet synchronous machines with aiding from estimation of rotor PM flux linkage," *IEEE Trans. Ind. Appl.*, vol. 51, no. 4, pp. 3115–3125, Jul./Aug. 2015.

[36] K. Liu, C. Hou, and W. Hua, "A novel inertia identification method and its application in PI controllers of PMSM drives," *IEEE Access*, vol. 7, pp. 13445–13454, 2019.

[37] M. A. Hamida, J. De Leon, A. Glumineau, and R. Boisliveau, "An adaptive interconnected observer for sensorless control of PM synchronous motors with online parameter identification," *IEEE Trans. Ind. Electron.*, vol. 60, no. 2, pp. 739–748, Feb. 2013.

[38] G. Zhu, L.-A. Dessaint, O. Akhrif, and A. Kaddouri, "Speed tracking control of a permanent-magnet synchronous motor with state and load torque observer," *IEEE Trans. Ind. Electron.*, vol. 47, no. 2, pp. 346–355, Apr. 2000.

[39] Y. Yan, J. Yang, Z. Sun, C. Zhang, S. Li, and H. Yu, "Robust speed regulation for PMSM servo system with multiple sources of disturbances via an augmented disturbance observer," *IEEE/ASME Trans. Mechatronics*, vol. 23, no. 2, pp. 769–780, Apr. 2018.

[40] X. Zhang and Z. Li, "Sliding-mode observer-based mechanical parameter estimation for permanent magnet synchronous motor," *IEEE Trans. Power Electron.*, vol. 31, no. 8, pp. 5732–5745, Aug. 2016.

[41] Y. Feng, X. Yu, and F. Han, "High-order terminal sliding-mode observer for parameter estimation of a permanent-magnet synchronous motor," *IEEE Trans. Ind. Electron.*, vol. 60, no. 10, pp. 4272–4280, Oct. 2013.

[42] C. Lian, F. Xiao, S. Gao, and J. Liu, "Load torque and moment of inertia identification for permanent magnet synchronous motor drives based on sliding mode observer," *IEEE Trans. Power Electron.*, vol. 34, no. 6, pp. 5675–5683, Jun. 2019.

[43] W. Lu, B. Tang, K. Ji, K. Lu, D. Wang, and Z. Yu, "A new load adaptive identification method based on an improved sliding mode observer for PMSM position servo system," *IEEE Trans. Power Electron.*, vol. 36, no. 3, pp. 3211–3223, Mar. 2021.

[44] M. S. Rafaq and J.-W. Jung, "A comprehensive review of state-of-the-art parameter estimation techniques for permanent magnet synchronous motors in wide speed range," *IEEE Trans. Ind. Informat.*, vol. 16, no. 7, pp. 4747–4758, Jul. 2020.

[45] H. Ahn, H. Park, C. Kim, and H. Lee, "A review of state-of-the-art techniques for PMSM parameter identification," *J. Electr. Eng. Technol.*, vol. 15, no. 3, pp. 1177–1187, Mar. 2020.

[46] B. Stumberger, G. Stumberger, D. Dolinar, A. Hamler, and M. Trlep, "Evaluation of saturation and cross-magnetization effects in interior permanent-magnet synchronous motor," *IEEE Trans. Ind. Appl.*, vol. 39, no. 5, pp. 1264–1271, Sep./Oct. 2003.

[47] N. A. Demerdash, T. M. Hijazi, and A. A. Arkadan, "Computation of winding inductances of permanent magnet brushless DC motors with damper windings by energy perturbation," *IEEE Trans. Energy Convers.*, vol. EC-3, no. 3, pp. 705–713, Sep. 1988.

[48] T. W. Nehl, F. A. Fouad, and N. A. Demerdash, "Determination of saturated values of rotating machinery incremental and apparent inductances by an energy perturbation method," *IEEE Power Eng. Rev.*, vol. PER-2, no. 12, pp. 28–29, Dec. 1982.

[49] Y. S. Chen, "Motor topologies and control strategies for permanent magnet brushless AC drives," Ph.D. dissertation, Univ. Sheffield, Sheffield, U.K., 1999.

[50] F. Khatounian, S. Moreau, E. Monmasson, A. Janot, and F. Louveau, "Parameters estimation of the actuator used in haptic interfaces: Comparison of two identification methods," in *Proc. IEEE Int. Symp. Ind. Electron.*, vol. 1, Jul. 2006, pp. 211–216.

[51] K. M. Rahman and S. Hiti, "Identification of machine parameters of a synchronous motor," *IEEE Trans. Ind. Appl.*, vol. 41, no. 2, pp. 557–565, Mar. 2005.

[52] S. A. Odhano, R. Bojoi, S. G. Rosu, and A. Tenconi, "Identification of the magnetic model of permanent-magnet synchronous machines using DC-biased low-frequency AC signal injection," *IEEE Trans. Ind. Appl.*, vol. 51, no. 4, pp. 3208–3215, Jul. 2015.

[53] B. Stumberger, B. Kreca, and B. Hribernik, "Determination of parameters of synchronous motor with permanent magnets from measurement of load conditions," *IEEE Trans. Energy Convers.*, vol. 14, no. 4, pp. 1413–1416, Dec. 1999.

[54] B. J. Chalmers, S. A. Hamed, and G. D. Baines, "Parameters and performance of a high-field permanent-magnet synchronous motor for variable-frequency operation," *IEE Proc. B, Electr. Power Appl.*, vol. 132, no. 3, p. 117, 1985.

[55] E. Armando, R. I. Bojoi, P. Guglielmi, G. Pellegrino, and M. Pastorelli, "Experimental identification of the magnetic model of synchronous machines," *IEEE Trans. Ind. Appl.*, vol. 49, no. 5, pp. 2116–2125, Sep. 2013.

[56] G. Pellegrino, B. Boazzo, and T. M. Jahns, "Magnetic model self-identification for PM synchronous machine drives," *IEEE Trans. Ind. Appl.*, vol. 51, no. 3, pp. 2246–2254, May/Jun. 2015.

[57] K. Liu, J. Feng, S. Guo, L. Xiao, and Z.-Q. Zhu, "Identification of flux linkage map of permanent magnet synchronous machines under uncertain circuit resistance and inverter nonlinearity," *IEEE Trans. Ind. Informat.*, vol. 14, no. 2, pp. 556–568, Feb. 2018.

[58] M. Rashed, P. F. A. MacConnell, A. F. Stronach, and P. Acarnley, "Sensorless indirect-rotor-field-orientation speed control of a permanent-magnet synchronous motor with stator-resistance estimation," *IEEE Trans. Ind. Electron.*, vol. 54, no. 3, pp. 1664–1675, Jun. 2007.

[59] S. Morimoto, M. Sanada, and Y. Takeda, "Mechanical sensorless drives of IPMSM with online parameter identification," *IEEE Trans. Ind. Appl.*, vol. 42, no. 5, pp. 1241–1248, Sep./Oct. 2006.

[60] S.-B. Lee, "Closed-loop estimation of permanent magnet synchronous motor parameters by PI controller gain tuning," *IEEE Trans. Energy Convers.*, vol. 21, no. 4, pp. 863–870, Dec. 2006.

[61] K. Liu, Q. Zhang, J. Chen, Z. Q. Zhu, and J. Zhang, "Online multi-parameter estimation of nonsalient-pole PM synchronous machines with temperature variation tracking," *IEEE Trans. Ind. Electron.*, vol. 58, no. 5, pp. 1776–1788, May 2011.

[62] K. Liu, Z. Q. Zhu, and D. A. Stone, "Parameter estimation for condition monitoring of PMSM stator winding and rotor permanent magnets," *IEEE Trans. Ind. Electron.*, vol. 60, no. 12, pp. 5902–5913, Dec. 2013.

[63] Z.-H. Liu, H.-L. Wei, X.-H. Li, K. Liu, and Q.-C. Zhong, "Global identification of electrical and mechanical parameters in PMSM drive based on dynamic self-learning PSO," *IEEE Trans. Power Electron.*, vol. 33, no. 12, pp. 10858–10871, Dec. 2018.

[64] K. Liu, Z. Q. Zhu, Q. Zhang, and J. Zhang, "Influence of nonideal voltage measurement on parameter estimation in permanent-magnet synchronous machines," *IEEE Trans. Ind. Electron.*, vol. 59, no. 6, pp. 2438–2447, Jun. 2012.

[65] K. Liu and Z. Q. Zhu, "Online estimation of the rotor flux linkage and voltage-source inverter nonlinearity in permanent magnet synchronous machine drives," *IEEE Trans. Power Electron.*, vol. 29, no. 1, pp. 418–427, Jan. 2014.

[66] K. Liu and Z. Q. Zhu, "Position-offset-based parameter estimation using the Adaline NN for condition monitoring of permanent-magnet synchronous machines," *IEEE Trans. Ind. Electron.*, vol. 62, no. 4, pp. 2372–2383, Apr. 2015.

[67] Y. Qi, E. Bostanci, V. Gurusamy, and B. Akin, "A comprehensive analysis of short-circuit current behavior in PMSM interturn short-circuit faults," *IEEE Trans. Power Electron.*, vol. 33, no. 12, pp. 10784–10793, Dec. 2018.

[68] Y. Zhang, G. Liu, W. Zhao, H. Zhou, Q. Chen, and M. Wei, "Online diagnosis of slight interturn short-circuit fault for a low-speed permanent magnet synchronous motor," *IEEE Trans. Transport. Electrific.*, vol. 7, no. 1, pp. 104–113, Mar. 2021.

[69] K.-H. Kim, "Simple online fault detecting scheme for short-circuited turn in a PMSM through current harmonic monitoring," *IEEE Trans. Ind. Electron.*, vol. 58, no. 6, pp. 2565–2568, Jun. 2011.

[70] M. A. Mazzoletti, G. R. Bossio, C. H. De Angelo, and D. R. Espinoza-Trejo, "A model-based strategy for interturn short-circuit fault diagnosis in PMSM," *IEEE Trans. Ind. Electron.*, vol. 64, no. 9, pp. 7218–7228, Sep. 2017.

[71] J. Hang, J. Zhang, M. Xia, S. Ding, and W. Hua, "Interturn fault diagnosis for model-predictive-controlled-PMSM based on cost function and wavelet transform," *IEEE Trans. Power Electron.*, vol. 35, no. 6, pp. 6405–6418, Jun. 2020.

[72] Z.-H. Liu, J. Zhang, S.-W. Zhou, X.-H. Li, and K. Liu, "Coevolutionary particle swarm optimization using AIS and its application in multiparameter estimation of PMSM," *IEEE Trans. Cybern.*, vol. 43, no. 6, pp. 1921–1935, Dec. 2013.
[73] Z.-H. Liu, X.-H. Li, L.-H. Wu, S.-W. Zhou, and K. Liu, "GPU-accelerated parallel coevolutionary algorithm for parameters identification and temperature monitoring in permanent magnet synchronous machines," *IEEE Trans. Ind. Informat.*, vol. 11, no. 5, pp. 1220–1230, Oct. 2015.
[74] K.-W. Lee, D.-H. Jung, and I.-J. Ha, "An online identification method for both stator resistance and back-EMF coefficient of PMSMs without rotational transducers," *IEEE Trans. Ind. Electron.*, vol. 51, no. 2, pp. 507–510, Apr. 2004.
[75] G. Feng, C. Lai, and N. C. Kar, "A novel current injection-based online parameter estimation method for PMSMs considering magnetic saturation," *IEEE Trans. Magn.*, vol. 52, no. 7, pp. 1–4, Jul. 2016.
[76] G. Feng, C. Lai, K. Mukherjee, and N. C. Kar, "Current injection-based online parameter and VSI nonlinearity estimation for PMSM drives using current and voltage DC components," *IEEE Trans. Transport. Electrific.*, vol. 2, no. 2, pp. 119–128, Jun. 2016.
[77] C. Lai, G. Feng, K. Mukherjee, V. Loukanov, and N. C. Kar, "Torque ripple minimization for interior PMSM with consideration of magnetic saturation incorporating online parameter identification," *IEEE Trans. Magn.*, vol. 53, no. 6, pp. 1–4, Jun. 2017.
[78] S. D. Wilson, P. Stewart, and B. P. Taylor, "Methods of resistance estimation in permanent magnet synchronous motors for real-time thermal management," *IEEE Trans. Energy Convers.*, vol. 25, no. 3, pp. 698–707, Sep. 2010.
[79] S. Wilson, P. Stewart, and J. Stewart, "Real-time thermal management of permanent magnet synchronous motors by resistance estimation," *IET Electr. Power Appl.*, vol. 6, no. 9, pp. 716–726, Nov. 2012.
[80] K. Liu and Z. Q. Zhu, "Quantum genetic algorithm-based parameter estimation of PMSM under variable speed control accounting for system identifiability and VSI nonlinearity," *IEEE Trans. Ind. Electron.*, vol. 62, no. 4, pp. 2363–2371, Apr. 2015.
[81] K. Liu and Z. Q. Zhu, "Position offset-based parameter estimation for permanent magnet synchronous machines under variable speed control," *IEEE Trans. Power Electron.*, vol. 30, no. 6, pp. 3438–3446, Jun. 2015.
[82] D. D. Reigosa, P. Garcia, F. Briz, D. Raca, and R. D. Lorenz, "Modeling and adaptive decoupling of high-frequency resistance and temperature effects in carrier-based sensorless control of PM synchronous machines," *IEEE Trans. Ind. Appl.*, vol. 46, no. 1, pp. 139–149, Jul. 2010.
[83] D. Reigosa, D. Fernández, M. Martínez, J. M. Guerrero, A. B. Diez, and F. Briz, "Magnet temperature estimation in permanent magnet synchronous machines using the high frequency inductance," *IEEE Trans. Ind. Appl.*, vol. 55, no. 3, pp. 2750–2757, May 2019.
[84] M. Martinez, D. Reigosa, D. Fernandez, J. M. Guerrero, and F. Briz, "Enhancement of permanent-magnet synchronous machines torque estimation using pulsating high-frequency current injection," *IEEE Trans. Ind. Appl.*, vol. 56, no. 1, pp. 358–366, Jan./Feb. 2020.
[85] J. Zhou, K. Huang, S. Huang, S. Liu, H. Zhao, and M. Shen, "Inductance parameter identification method of permanent magnet synchronous motor based on the HF rotating square wave voltage injection," in *Proc. 22nd Int. Conf. Electr. Mach. Syst. (ICEMS)*, Aug. 2019, pp. 1–4.
[86] G. El-Murr, D. Giaouris, and J. W. Finch, "Online cross-coupling and self incremental inductances determination of salient permanent magnet synchronous machines," in *Proc. 5th IET Int. Conf. Power Electron., Mach. Drives (PEMD)*, 2010, pp. 1–4.
[87] D. Fernandez, D. Reigosa, T. Tanimoto, T. Kato, and F. Briz, "Wireless permanent magnet temperature & field distribution measurement system for IPMSMs," in *Proc. IEEE Energy Conv. Cong. Expo. (ECCE)*, Montreal, QC, Canada, Sep. 2015, pp. 3996–4003.
[88] D. D. Reigosa, F. Briz, P. García, J. M. Guerrero, and M. W. Degner, "Magnet temperature estimation in surface PM machines using high-frequency signal injection," *IEEE Trans. Ind. Appl.*, vol. 46, no. 4, pp. 1468–1475, Jul. 2010.
[89] B. Shuang and Z. Q. Zhu, "A novel method for measuring high frequency DQ-axis and cross-coupling inductances in interior permanent magnet synchronous machines," in *Proc. IEEE Energy Conv. Cong. Expo. (ECCE)*, Detroit, MI, USA, Oct. 2020, pp. 6096–6103.
[90] W. Xu and R. D. Lorenz, "High-frequency injection-based stator flux linkage and torque estimation for DB-DTFC implementation on IPMSMs considering cross-saturation effects," *IEEE Trans. Ind. Appl.*, vol. 50, no. 6, pp. 3805–3815, Nov./Dec. 2014.
[91] G. Wang, J. Kuang, N. Zhao, G. Zhang, and D. Xu, "Rotor position estimation of PMSM in low-speed region and standstill using zero-voltage vector injection," *IEEE Trans. Power Electron.*, vol. 33, no. 9, pp. 7948–7958, Sep. 2018.
[92] G. Xie, K. Lu, S. K. Dwivedi, R. J. Riber, and W. Wu, "Permanent magnet flux online estimation based on zero-voltage vector injection method," *IEEE Trans. Power Electron.*, vol. 30, no. 12, pp. 6506–6509, Dec. 2015.
[93] G. Feng, C. Lai, K. Mukherjee, and N. C. Kar, "Online PMSM magnet flux-linkage estimation for rotor magnet condition monitoring using measured speed harmonics," *IEEE Trans. Ind. Appl.*, vol. 53, no. 3, pp. 2786–2794, May/Jun. 2017.
[94] G. Feng, C. Lai, and N. C. Kar, "Particle-filter-based magnet flux linkage estimation for PMSM magnet condition monitoring using harmonics in machine speed," *IEEE Trans. Ind. Informat.*, vol. 13, no. 3, pp. 1280–1290, Jun. 2017.
[95] S. Ichikawa, M. Tomita, S. Doki, and S. Okuma, "Sensorless control of permanent-magnet synchronous motors using online parameter identification based on system identification theory," *IEEE Trans. Ind. Electron.*, vol. 53, no. 2, pp. 363–372, Apr. 2006.
[96] S. Moreau, R. Kahoul, and J.-P. Louis, "Parameters estimation of permanent magnet synchronous machine without adding extra-signal as input excitation," in *Proc. IEEE Int. Symp. Ind. Electron.*, vol. 1, May 2004, pp. 371–376.
[97] Y. Inoue, K. Yamada, S. Morimoto, and M. Sanada, "Effectiveness of voltage error compensation and parameter identification for model-based sensorless control of IPMSM," *IEEE Trans. Ind. Appl.*, vol. 45, no. 1, pp. 213–221, Jan./Feb. 2009.
[98] Y. Inoue, Y. Kawaguchi, S. Morimoto, and M. Sanada, "Performance improvement of sensorless IPMSM drives in a low-speed region using online parameter identification," *IEEE Trans. Ind. Appl.*, vol. 47, no. 2, pp. 798–804, Mar./Apr. 2011.
[99] S.-Y. Cho, W.-G. Shin, J.-S. Park, and W.-H. Kim, "A torque compensation control scheme of PMSM considering wide variation of permanent magnet temperature," *IEEE Trans. Magn.*, vol. 55, no. 2, pp. 1–5, Feb. 2019.
[100] X. Xiao, C. Chen, and M. Zhang, "Dynamic permanent magnet flux estimation of permanent magnet synchronous machines," *IEEE Trans. Appl. Supercond.*, vol. 20, no. 3, pp. 1085–1088, Jun. 2010.
[101] Y. Shi, K. Sun, L. Huang, and Y. Li, "Online identification of permanent magnet flux based on extended Kalman filter for IPMSM drive with position sensorless control," *IEEE Trans. Ind. Electron.*, vol. 59, no. 11, pp. 4169–4178, Nov. 2012.
[102] Z. Q. Zhu, X. Zhu, P. D. Sun, and D. Howe, "Estimation of winding resistance and PM flux-linkage in brushless AC machines by reduced-order extended Kalman filter," in *Proc. IEEE Int. Conf. Netw., Sens. Control*, London, U.K., Apr. 2007, pp. 740–745.
[103] L. Liu and D. A. Cartes, "Synchronisation based adaptive parameter identification for permanent magnet synchronous motors," *IET Control Theory Appl.*, vol. 1, no. 4, pp. 1015–1022, Jul. 2007.
[104] X. Xi, Z. Meng, L. Yongdong, and L. Min, "On-line estimation of permanent magnet flux linkage ripple for PMSM based on a Kalman filter," in *Proc. 32nd Annu. Conf. IEEE Ind. Electron. (IECON)*, Paris, France, Nov. 2006, pp. 1171–1175.
[105] T. Boileau, B. Nahid-Mobarakeh, and F. Meibody-Tabar, "On-line identification of PMSM parameters: Model-reference vs EKF," in *Proc. IEEE Ind. Appl. Soc. Annu. Meeting*, Edmonton, AB, Canada, Oct. 2008, pp. 1–8.
[106] B. N. Mobarakeh, F. Meibody-Tabar, and F. M. Sargos, "On-line identification of PMSM electrical parameters based on decoupling control," in *Proc. IEEE Ind. Appl. Soc. Annu. Meeting*, Chicago, IL, USA, vol. 1, Sep. /Oct. 2001, pp. 266–273.
[107] B. Nahid-Mobarakeh, F. Meibody-Tabar, and F.-M. Sargos, "Mechanical sensorless control of PMSM with online estimation of stator resistance," *IEEE Trans. Ind. Appl.*, vol. 40, no. 2, pp. 457–471, Mar./Apr. 2004.
[108] S. J. Underwood and I. Husain, "Online parameter estimation and adaptive control of permanent-magnet synchronous machines," *IEEE Trans. Ind. Electron.*, vol. 57, no. 7, pp. 2435–2443, Jul. 2010.
[109] A. Piippo, M. Hinkkanen, and J. Luomi, "Adaptation of motor parameters in sensorless PMSM drives," *IEEE Trans. Ind. Appl.*, vol. 45, no. 1, pp. 203–212, Jan./Feb. 2009.
[110] D. D. Reigosa, F. Briz, M. W. Degner, P. Garcia, and J. M. Guerrero, "Temperature issues in saliency-tracking-based sensorless methods for PM synchronous machines," *IEEE Trans. Ind. Appl.*, vol. 47, no. 3, pp. 1352–1360, May/Jun. 2011.

[111] M. Burth, G. C. Verghese, and M. Velez-Reyes, "Subset selection for improved parameter estimation in on-line identification of a synchronous generator," *IEEE Trans. Power Syst.*, vol. 14, no. 1, pp. 218–225, Feb. 1999.
[112] C. E. Nino and M. Velez-Reyes, "Dealing with ill conditioning in recursive parameter estimation for a synchronous generator," in *Proc. 32nd Annu. Conf. IEEE Ind. Electron. (IECON)*, Paris, France, Nov. 2006, pp. 1089–1094.
[113] H.-W. Kim, M.-J. Youn, K.-Y. Cho, and H.-S. Kim, "Nonlinearity estimation and compensation of PWM VSI for PMSM under resistance and flux linkage uncertainty," *IEEE Trans. Control Syst. Technol.*, vol. 14, no. 4, pp. 589–601, Jul. 2006.
[114] J.-W. Choi and S.-K. Sul, "Inverter output voltage synthesis using novel dead time compensation," *IEEE Trans. Power Electron.*, vol. 11, no. 2, pp. 221–227, Mar. 1996.
[115] T.-C. Lee, Y. Tan, and D. Nesic, "Stability and persistent excitation in signal sets," *IEEE Trans. Autom. Control*, vol. 60, no. 5, pp. 1188–1203, May 2015.
[116] K. Liu, "Research on the online multi-parameter identification of permanent magnet synchronous machines," Ph.D. dissertation, Hunan Univ., Changsha, China, 2010.
[117] G. Feng, C. Lai, J. Tjong, and N. C. Kar, "Noninvasive Kalman filter based permanent magnet temperature estimation for permanent magnet synchronous machines," *IEEE Trans. Power Electron.*, vol. 33, no. 12, pp. 10673–10682, Dec. 2018.
[118] S. Xiao and A. Griffo, "PWM-based flux linkage and rotor temperature estimations for permanent magnet synchronous machines," *IEEE Trans. Power Electron.*, vol. 35, no. 6, pp. 6061–6069, Jun. 2020.
[119] T. Senjyu, K. Kinjo, N. Urasaki, and K. Uezato, "Parameter measurement for PMSM using adaptive identification," in *Proc. IEEE Int. Symp. Ind. Electron.*, L'Aquila, Italy, vol. 3, Jul. 2002, pp. 711–716.
[120] O. C. Kivanc and S. B. Ozturk, "Sensorless PMSM drive based on stator feedforward voltage estimation improved with MRAS multiparameter estimation," *IEEE/ASME Trans. Mechatronics*, vol. 23, no. 3, pp. 1326–1337, Jun. 2018.
[121] Z. Chen, M. Tomita, S. Doki, and S. Okuma, "An extended electromotive force model for sensorless control of interior permanent-magnet synchronous motors," *IEEE Trans. Ind. Electron.*, vol. 50, no. 2, pp. 288–295, Apr. 2003.
[122] M. Hinkkanen, T. Tuovinen, L. Harnefors, and J. Luomi, "A combined position and stator-resistance observer for salient PMSM drives: Design and stability analysis," *IEEE Trans. Power Electron.*, vol. 27, no. 2, pp. 601–609, Feb. 2012.
[123] M. Hasegawa and K. Matsui, "Position sensorless control for interior permanent magnet synchronous motor using adaptive flux observer with inductance identification," *IET Elect. Power Appl.*, vol. 3, no. 3, pp. 209–217, May 2009.
[124] R. Raja, T. Sebastian, and M. Wang, "Online stator inductance estimation for permanent magnet motors using PWM excitation," *IEEE Trans. Transport. Electrific.*, vol. 5, no. 1, pp. 107–117, Mar. 2019.
[125] L. M. Gong and Z. Q. Zhu, "A novel method for compensating inverter nonlinearity effects in carrier signal injection-based sensorless control from positive-sequence carrier current distortion," *IEEE Trans. Ind. Appl.*, vol. 47, no. 3, pp. 1283–1292, May/Jun. 2011.
[126] P. Guglielmi, M. Pastorelli, and A. Vagati, "Cross saturation effects in IPM motors and related impact on zero-speed sensorless control," in *Proc. IEEE IAS Annu. Meeting*, vol. 4, Oct. 2005, pp. 2546–2552.
[127] Y. Li, Z. Q. Zhu, D. Howe, C. M. Bingham, and D. A. Stone, "Improved rotor-position estimation by signal injection in brushless AC motors, accounting for cross-coupling magnetic saturation," *IEEE Trans. Ind. Appl.*, vol. 45, no. 5, pp. 1843–1850, Sept./Oct. 2009.
[128] S. Liu and G. E. Kuhl, "Temperature coefficients of rare earth permanent magnets," *IEEE Trans. Magn.*, vol. 35, no. 5, pp. 3271–3273, Sep. 1999.
[129] S. Mortazavizadeh and M. Mousavi, "A review on condition monitoring and diagnostic techniques of rotating electric machines," *Phys. Sci. Int. J.*, vol. 4, no. 3, pp. 310–338, May 2014.
[130] H. Zhan and Z. Q. Zhu, "Nonintrusive online rotor permanent magnet temperature tracking for permanent magnet synchronous machine based on third harmonic voltage," in *Proc. IEEE Energy Conv. Congr. Expo.*, Milwaukee, WI, USA, Sep. 2016, pp. 1–8.
[131] M. Ganchev, H. Umschaden, and H. Kapeller, "Rotor temperature distribution measuring system," in *Proc. 37th Annu. Conf. IEEE Ind. Electron. Soc. (IECON)*, Melbourne, VIC, Australia, Nov. 2011, pp. 2006–2011.
[132] C. Mejuto, M. Mueller, M. Shanel, A. Mebarki, M. Reekie, and D. Staton, "Improved synchronous machine thermal modelling," in *Proc. 18th Int. Conf. Electr. Mach.*, Sep. 2008, pp. 1–6.
[133] X. Li and R. Kennel, "General formulation of Kalman-filter-based online parameter identification methods for VSI-fed PMSM," *IEEE Trans. Ind. Electron.*, vol. 68, no. 4, pp. 2856–2864, Apr. 2021.
[134] O. Wallscheid, A. Specht, and J. Böcker, "Observing the permanent-magnet temperature of synchronous motors based on electrical fundamental wave model quantities," *IEEE Trans. Ind. Electron.*, vol. 64, no. 5, pp. 3921–3929, May 2017.
[135] Y. Park, D. Fernandez, S. B. Lee, D. Hyun, M. Jeong, S. K. Kommuri, C. Cho, D. D. Reigosa, and F. Briz, "Online detection of rotor eccentricity and demagnetization faults in PMSMs based on Hall-effect field sensor measurements," *IEEE Trans. Ind. Appl.*, vol. 55, no. 3, pp. 2499–2509, May/Jun. 2019.
[136] R. R. Schoen, B. K. Lin, T. G. Habetler, J. H. Schlag, and S. Farag, "An unsupervised, on-line system for induction motor fault detection using stator current monitoring," *IEEE Trans. Ind. Appl.*, vol. 31, no. 6, pp. 1280–1286, Nov./Dec. 1995.
[137] B. Trajin, J. Regnier, and J. Faucher, "Detection of bearing faults in asynchronous motors using Luenberger speed observer," in *Proc. 34th Annu. Conf. IEEE Ind. Electron.*, Orlando, FL, USA, Nov. 2008, pp. 3073–3078.
[138] E. Ifeachor and B. Jervis, *Digital Signal Processing*, 2nd ed. Harlow, U.K.: Addison Wesley, 2002.
[139] A. H. Sayed and T. Kailath, "A state-space approach to adaptive RLS filtering," *IEEE Signal Process. Mag.*, vol. 11, no. 3, pp. 18–60, Jul. 1994.
[140] F. Auger, M. Hilairet, J. M. Guerrero, E. Monmasson, T. Orlowska-Kowalska, and S. Katsura, "Industrial applications of the Kalman filter: A review," *IEEE Trans. Ind. Electron.*, vol. 60, no. 12, pp. 5458–5471, Dec. 2013.
[141] K. Liu, Q. Zhang, Z.-Q. Zhu, J. Zhang, A.-W. Shen, and P. Stewart, "Comparison of two novel MRAS based strategies for identifying parameters in permanent magnet synchronous motors," *Int. J. Autom. Comput.*, vol. 7, no. 4, pp. 516–524, Nov. 2010.
[142] J. Kennedy and R. Eberhart, "Particle swarm optimization," in *Proc. IEEE Int. Neural Netw.*, Perth, WA, Australia, vol. 4, Nov./Dec. 1995, pp. 1942–1948.
[143] B. Widrow and M. A. Lehr, "30 years of adaptive neural networks: Perceptron, madaline, and backpropagation," *Proc. IEEE*, vol. 78, no. 9, pp. 1415–1442, Sep. 1990.
[144] K.-H. Han and J.-H. Kim, "Quantum-inspired evolutionary algorithm for a class of combinatorial optimization," *IEEE Trans. Evol. Comput.*, vol. 6, no. 6, pp. 580–593, Dec. 2002.
[145] A. Malossini, E. Blanzieri, and T. Calarco, "Quantum genetic optimization," *IEEE Trans. Evol. Comput.*, vol. 12, no. 2, pp. 231–241, Apr. 2008.
[146] W.-H. Chen, J. Yang, L. Guo, and S. Li, "Disturbance-observer-based control and related methods—An overview," *IEEE Trans. Ind. Electron.*, vol. 63, no. 2, pp. 1083–1095, Feb. 2016.
[147] K. D. Young, V. I. Utkin, and U. Ozguner, "A control engineer's guide to sliding mode control," *IEEE Trans. Control Syst. Technol.*, vol. 7, no. 3, pp. 328–342, May 1999.
[148] H. Kim, J. Son, and J. Lee, "A high-speed sliding-mode observer for the sensorless speed control of a PMSM," *IEEE Trans. Ind. Electron.*, vol. 58, no. 9, pp. 4069–4077, Sep. 2011.

Z. Q. ZHU (Fellow, IEEE) received the B.Eng. and M.Sc. degrees in electrical engineering from Zhejiang University, Hangzhou, China, in 1982 and 1984, respectively, and the Ph.D. degree in electrical engineering from The University of Sheffield, Sheffield, U.K., in 1991.

Since 1988, he has been with The University of Sheffield, where he has been a Professor with the Department of Electronic and Electrical Engineering, since 2000. He is currently the Royal Academy of Engineering/Siemens Research Chair, and the Head of the Electrical Machines and Drives Research Group, the Academic Director of the Sheffield Siemens Gamesa Renewable Energy Research Centre, the Director of the CRRC Electric Drives Technology Research Centre, and the Director of the Midea Electrical Machines and Control Systems Research Centre. His current research interests include the design and control of permanent magnet machines and drives for applications ranging from electric vehicles through domestic appliance to renewable energy. He is a Fellow of the Royal Academy of Engineering, U.K. He was a recipient of the 2021 IEEE Nikola Tesla Award and the 2019 IEEE IAS Outstanding Achievement Award.

DAWEI LIANG received the B.Eng. degree in electrical engineering from the Harbin Institute of Technology, Harbin, China, in 2014, and the M.Sc. degree in electrical engineering from the Karlsruhe Institute of Technology, Karlsruhe, Germany, in 2018. He is currently pursuing the Ph.D. degree with The University of Sheffield, Sheffield, U.K. His major research interests include thermal modeling and thermal management of electrical machines.

KAN LIU (Senior Member, IEEE) received the B.Eng. and Ph.D. degrees in automation from Hunan University, China, in 2005 and 2011, respectively, and the Ph.D. degree in electronic and electrical engineering from The University of Sheffield, Sheffield, U.K., in 2013.

From 2013 to 2016, he was a Research Associate with the Department of Electronic and Electrical Engineering, The University of Sheffield. From 2016 to 2017, he was a Lecturer with the Control Systems Group, Loughborough University. He is currently a Professor of electro-mechanical engineering and the Director of the Engineering Research Center of Automotive Electronics and Control Technology, Ministry of Education, Hunan University. His research interests include parameter estimation and sensorless control of permanent magnet synchronous machine drives, for applications ranging from automotive engineering to servo systems. He also serves as an Associate Editor for IEEE Access and the *CES Transactions on Electrical Machines and Systems*.